UNIVERSITÀ
DEGLI STUDI
DI FERRARA
- EX LABORE FRUCTUS -

Performance Optimization of Luminescent Solar Concentrator Photovoltaic Systems

Candidate:

Paolo Bernardoni

Supervisors:

Prof. Vincenzo Guidi

Prof. Donato Vincenzi

Index

1 Introduction

The purpose of this work is the optimization of photovoltaic systems based on luminescent solar concentrators, these devices [1] represent a promising technology that can be used to develop photovoltaic systems for building integration but, so far, a thorough analysis of the performance of LSC systems with sizes practical for building integration applications is missing.

In this work the performances of LSCs based on different dyes, different sizes and various optical configurations are analysed as well as the effect of self-absorption on the output spectrum.

Moreover the performances of the systems with different optical configurations are analysed under some possible shading conditions in order to identify the most efficient and convenient design non only under an ideal working exposure but also in real world far from ideal conditions.

The prototypes were built after an extensive work of simulation of their optical behaviour aimed at selecting the most promising designs, in particular non only the efficiency has been taken into account but also the scalability of the modules to larger or smaller sizes and the ease of assembly: important features for a design that should undergo a technology transfer from research to industrialization.

This thesis required a work in various research fields ranging from the operation theory of the concentrators and the programming of optical simulations to more experimental fields as the construction of prototypes, their characterization and installation in various operative environments.

1.1 Solar energy

The continuous increase in the world energy demand, largely satisfied by fossil fuels, and the effects that the emissions of carbon dioxide and other pollutants have on the global climate has fostered investments on the development of renewable energy sources and even oil companies are diversifying their business investing in renewable sources like BP with BP-Solar (now closed) and Total with SunPower.

At present the global requirements of electric energy are satisfied by less than 1% through solar technologies [2] despite the amount of energy provided by the sun in one year is 10^4 times higher than our global energy consumption.

There are various technologies aimed at the exploitation of solar energy, from low temperature applications like solar water heating used to provide hot water for domestic use to direct photovoltaic conversion of the solar energy into electricity and high

temperature applications like in concentrated solar power plants that use the sun as a heat source that is converted into electric energy through thermophotovoltaic generators or alternators coupled with turbines or Stirling engines.

Among these technologies the photovoltaic conversion is particularly interesting because permits a direct conversion to electricity, the scalability of the system from a single panel to a many MW size (579MW Solar Star project by SunPower [3] and the huge gap between the present efficiency and the theoretical limits of the photovoltaic conversion that leaves plenty of room for future developments.

1.2 Building integration

Photovoltaic and low temperature thermal solar panels, because of their scalability down to a small size, are commonly installed on the roof of the buildings to provide electricity and hot water and in case of remote sites can even satisfy all the energy consumption of the building (off-grid systems).

Most installations of this type are made with standard solar modules designed to be installed on the ground or on the roof without a tight integration into the structure and the design of the building.

This approach can be satisfactory as a low cost upgrade of existing buildings but is far from ideal for new constructions especially when aesthetic requirements must be fulfilled, in this case the use of the so called Building Integrated PhotoVoltaic (BIPV) modules is more appropriate because these devices are specifically designed to be deeply integrated into the structure of the buildings, stand out as architectural features and often can work properly even if installed on vertical surfaces.

In particular, in countries with a high population density where the surface available for large size photovoltaic power plants is limited, the power production of the systems integrated into the buildings can be significant and helps to avoid overload situations in the power network due to the coincidence of the points where production and consumption take place.

As noted before, the definition of building integration is not only relative to the physical installation of the photovoltaic systems in the building but concerns also the appealing design of the modules and the overall aesthetic appearance of the building.

It can be stated that building integrated systems are not installed *on* the building but *in* the building to underline their tight integration in the architectural design and, sometimes, even in the structural elements of the building.

Typically these devices are designed as solar windows or louvres, cladding of external

surfaces, tiles or paving stones that absorb the solar radiation and produce energy that is utilized by the building, the production exceeding the building consumption can be stored for overnight use or sold to the local power company.

The higher cost of these systems with respect to conventional modules is counterbalanced by their features both aesthetically (better appearance of the building) and technically (i.e. reduction in the summer air conditioning requirements), moreover they replace some building elements so the cost of the traditional building elements must be detracted from their cost).

Since building integrated modules and their mounting systems replace traditional construction elements, depending on their placement they must fulfil some more requirements with respect to traditional modules:

- Waterproofing of the building

- Mechanical resistance comparable to the replaced elements

- Thermal resistance comparable to the replaced elements

The building integration of the modules is complete if, after the removal of the modules, the functionality of the building skin is compromised, making the building not anymore suitable to use.

Photovoltaic systems can be integrated in buildings at the time of their construction or renovation and in this way is possible to fully optimise the aesthetic and installation aspects of the project, otherwise is possible to retrofit an existing building but in this case at the cost of a higher design complexity because in the existing building is probably lacking the electric system needed to connect the modules and proper structures to host them. In this case is rarely possible to achieve a full integration and an ideal orientation of the modules that are typically installed on an additional framework placed on the structure.

There are three main categories of photovoltaic panels for building integrations, depending on the part of the building where they are installed we can identify:

- Modules installed on roofs or horizontal surfaces, these are the most common and can effectively replace a traditional roof covers. Solar roof tiles and shingles are available to retrofit buildings whose traditional appearance must be preserved.

- Modules installed on walls and other vertical surfaces, these modules can be integrated into cladding panels that provide also a thermal insulation layer (full integration) or can be placed on external structures to achieve a more optimal orientation.

- Transparent modules intended to replace windows or skylights both in vertical and horizontal applications, these modules when integrated into a double glazing structure can substitute the existing windows with minimal modifications.

2 Luminescent Solar Concentrators

Within concentrating photovoltaic (CPV) systems, luminescent solar concentrators (LSC) combine energy production with pleasant aesthetic features allowing to be used in architectural solutions, in particular LSCs are, to date, one of the few technologies allowing the creation of transparent photovoltaic panels that do not distort or fog the image observed through the panel.

For various reasons luminescent solar concentrators (LSCs) represent a very attractive concept for a concentrating photovoltaic system [4]:

- low cost energy production (the quantity of solar cells needed for a given power output is strongly reduced);
- LSCs operate both with direct and diffuse light, therefore not needing expensive solar tracking devices;
- only ‘cold’ light is collected by the PV-cells, resulting in higher photovoltaic conversion efficiency;
- Filtering of dangerous UV radiation, due to strong absorption of the dyes in this spectrum;

Unlike most concentrating photovoltaic devices LSCs do not require expensive solar tracking and are made predominantly of plastic thus reducing the final cost and simplifying their architectural integration, moreover LSCs are able to convert effectively also the diffuse component of solar radiation allowing their use both in vertical arrangement (i.e. glass façades) and in situations without direct sun exposure (i.e. north-exposed façades).

LSC panels are constituted by a transparent dye-functionalized slab (the proper LSC device) coupled with small-size photovoltaic cells, the solar light incident on the slab is absorbed by the dyes, re-emitted inside the slab that acts as a waveguide and finally collected by solar cells mounted at the perimeter of the slab (see Fig. 2.1).

As their name implies LSCs are devices that concentrate light: the key principle is that the light emitted inside a medium with a refractive index higher than air and impinging on the surface of separation between this medium and the air has a so-called critical angle of incidence above what the light is not refracted but reflected back with a theoretical efficiency of 100% (the actual efficiency depends on the surface flatness).

This phenomenon is called total internal reflection and is often exploited to allow the propagation of light for long distances with minimum losses like in optic fibres, in fact the best dielectric mirrors can achieve a reflectivity as high as 99% in the visible spectrum but even with a so high reflectivity the amount of light surviving after just 10 reflections would

be roughly 90% therefore in order to permit an efficient light transport the total internal reflection is mandatory.

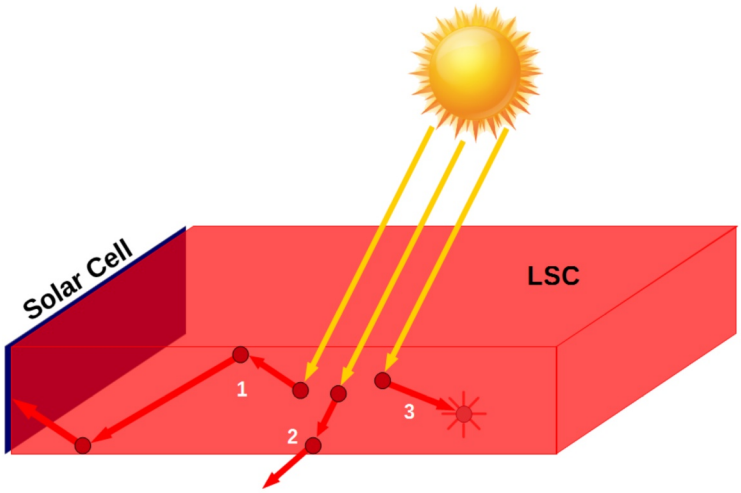

Fig. 2.1: In LSCs three phenomena can occur when a solar photon is absorbed by the dye: (1) the re-emitted radiation is above the critical angle so is trapped inside the slab until is absorbed by the cells, (2) the re-emitted radiation is emitted below the critical angle and it is lost, (3) the emitted radiation is absorbed by another dye molecule (self absorption).

The remaining part of the re-emitted light is lost through the surfaces of the slabs giving them their characteristic colour (see Fig. 2.2).

The angle above which total internal reflection occurs depends on the refractive index of the transparent medium, according to Snell's law:

$$n_1 \sin(\theta_1) = n_2 \sin(\theta_2)$$

if the second medium is air ($n_2 \approx 1$) and solving for $\sin(\theta_1)$

$$\sin(\theta_1) = \frac{1}{n_1} \sin(\theta_2)$$

the critical angle is the angle of incidence that gives a refracted angle of $\pi/2$

$$\theta_{critical} = \arcsin\left(\frac{1}{n_1}\right)$$

For instance the polymethylmethacrylate (PMMA), a plastic commonly known as acrylic glass, has a refractive index of 1.488 so about 25% of the emitted light is lost through the faces of the slab: the relationship between the refractive index of the transparent medium and the optical efficiency of the concentrator is covered in detail in chapter 2.2 and in

Appendix A.

The LSC devices have typically the shape of slabs with a thickness of a few millimetres, so all the light collected by the LSC that undergoes total internal reflection is reflected by the two main surfaces until it reaches the sides, which surface is small compared to the area of the slab, achieving an optical concentration.

In order to get this effect in the LSC, the light must be emitted inside the transparent medium, this emission is obtained doping the optical medium with fluorescent dyes whose emission is collected and concentrated on the sides of the LSC.

These dyes (that can be organic or inorganic dyes [5] as well as quantum dots) act as luminescence centres in the slabs and work absorbing part of the sunlight passing through the LSC then re-emitting isotropically the absorbed energy as light at higher wavelengths (fluorescence).

Fig. 2.2: A detail showing the edge of an LSC slab fitted with the receivers and the reflective film on the side edges, later an aluminium profile filled with silicone sealant have been installed around the receivers in order to protect the cells and the electrical connections from water and dust.

One of the drawbacks of this phenomenon is that the absorption and emission spectra in most dyes present a partial overlap: therefore some of the emitted photons can be absorbed again by the dye as they travel through the LSC reducing the efficiency of the system because any time an absorption-emission occurs the associated emission is isotropic and leads to further escape cone losses.

The re-absorption phenomenon in the LSC is explained in chapter 2.1 while detailed measures of self absorption inside the LSCs can be found in chapter 5.1.

Since the LSC concentration depends both on their geometry and doping the concentration factor can be expressed as $C=G*\eta_{opt}$ [6] where G is the geometric ratio and η_{opt} is the optical efficiency. The geometric ratio is expressed as the area of the LSC surface exposed to sunlight divided by the area of the sides and therefore is dependant only on the shape of the system while η_{opt} is the ratio between the photons that reach the sides and the photons passing through the LSC and depends on the dye type and concentration.

In order to produce energy the LSC slabs must be coupled with photovoltaic cells, the fluorescent cover can be applied on top of conventional solar cells to increase their quantum efficiency al lower wavelengths shifting the blue-violet-UV spectrum towards the red-yellow spectrum where most cells have higher quantum efficiencies.

Anyway the most striking application of LSC is their use in transparent concentrators where the cells are placed on the sides of the slab and receive the light emitted by the fluorescent dyes and concentrated to an irradiance level that can reach 4-5 times the solar constant (1000W/m^2 at AM 1.5).

2.1 Characteristics of the fluorescent dyes

In order to be useful in photovoltaic applications a dye must have the following characteristics:

- Wide absorption spectrum
- Large Stokes shift
- High quantum yield
- Limited self-absorption
- Good blending into the transparent medium
- High stability when exposed to ultraviolet radiation

A wide absorption spectrum permits the conversion of a larger amount of sunlight because obviously only the light absorbed by the dye contributes to the energy production of the LSC, the absorption efficiency can be defined as the rate of sunlight that can be absorbed by the dye.

$$\eta_{abs}=\frac{I_{absorbed}}{I_{sun}}$$

In the process of fluorescence the emitted photons always have a longer wavelength (or lower energy since E=hc/λ) than the absorbed ones, this phenomenon known as Stokes Shift always causes an unavoidable energy loss even in dyes with a near unity quantum

efficiency.

The fraction of energy remaining after the fluorescence process

$$\eta_{Stokes} = \frac{\bar{E}_{emitted}}{\bar{E}_{absorbed}}$$

and the fluorescence quantum yield representing the probability of emission resulting from the absorption of a photon

$$\eta_{qy} = \frac{n_{emitted}}{n_{absorbed}}$$

are two parameters that contribute to the overall optical efficiency η_{opt}.

One of the key factors hindering LSC performances is self absorption: most dyes show an overlap in their emission and absorption spectra (see Fig. 2.1.1) so the dye itself absorbs part of the emitted light and each time an absorption-emission occurs its associated escape cone and quantum efficiency losses reduce the efficiency of the system η_{sa}.

The probability for a photon to be re-absorbed is a statistical process which depends on the concentration of the dye and the length of the optical path inside the LSC thus becoming a key factor in the choice of the LSC geometry and dye concentration.

The contribution of self-absorption to the overall optical efficiency η_{sa} can be expressed as the probability that has a generic photon to be absorbed throughout its path inside the LSC.

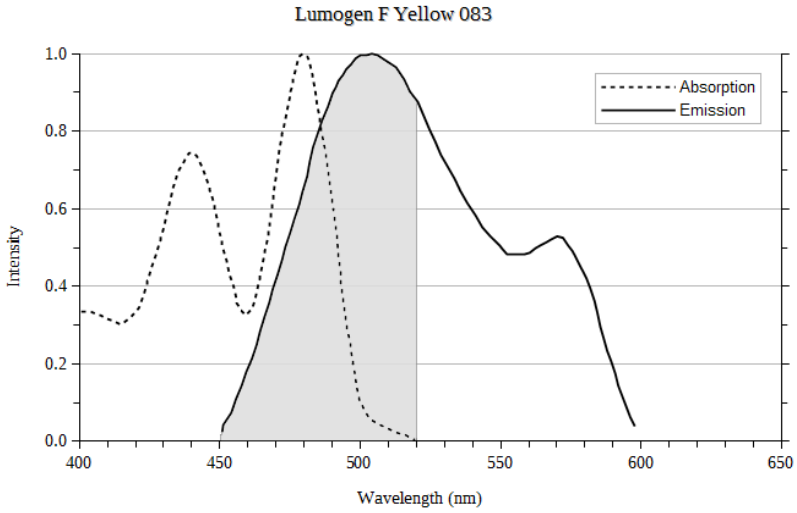

Fig. 2.1.1: Absorption and emission spectra of Lumogen F Yellow 083, the region painted in grey represents the portion of the emission spectrum that can be re-absorbed by the dye: in this case approximately half of the emitted spectrum can be lost due to self-absorption, leading to a low efficiency in LSCs with a large area or a high concentration of this dye.

In LSC three main categories of fluorescent dyes can be identified:

- Organic dyes
- Organometallic dyes
- Quantum dots

A high number of organic molecules exhibit fluorescence, these dyes are widely used in biology and medicine as markers in the study of cells and life beings but only a few of them are suitable to use in luminescent solar concentrators because of their sensitivity to ultraviolet radiation, low thermal stability or high cost.

The most stable compounds are widely used in the plastic industry as colouring agents because the emission connected to fluorescence gives them a particularly intense colour, moreover, being used in the manufacturing of plastics, these dyes are also the cheapest available.

In the following table are summarised the peculiar characteristics of four commercial organic dyes that were tested in this work.

Dye (Lumogen® F family)	*Type*	*Heat Stability (°C)*	*Absorption Peak (nm)*	*Emission Peak (nm)*	*Max Quantum Yield (nm)*

Violet 570	Naphtalimide	300	378	413	0.94
Yellow 083	Perylene	280	473	490	0.91
Orange 240	Perylene	300	525	539	0.99
Red 305	Perylene	300	578	613	0.98

Organometallic compounds are hybrid molecules where a metallic ion is bonded in an organic molecule, these metallic ions are typically lanthanides with $^{3+}$ oxidation [7] like europium (Eu^{3+} [8]), samarium (Sm^{3+}), terbium (Tb^{3+}), dysprosium (Dy^{3+}) and gadolinium (Gd^{3+}).

Quantum dots are the most promising materials for the future developments in the LSC technology, they consist in nanocrystals made of semiconductors which size is small enough (2-10nm) to affect the band structure due to quantum confinement [9], for this reason their electronic properties fall between those of a discrete molecule and bulk semiconductor.

The most striking feature of quantum dots is that their energy levels can be tuned precisely depending on the particle size and consequently is possible to choose the proper emission spectrum to maximize the efficiency of the cells or to make available a full spectrum of colours, moreover since quantum dots are made of inorganic semiconductors they have a muck higher thermal and optical stability with respect to organic dyes.

2.2 Influence of the optical medium

LSCs rely on total internal reflection to achieve their light concentration properties so, in principle, any transparent medium with a refractive index higher than air can be used for this purpose, however the use of mediums with a low refractive index would result in a significant increase in the light loss from the escape cone.

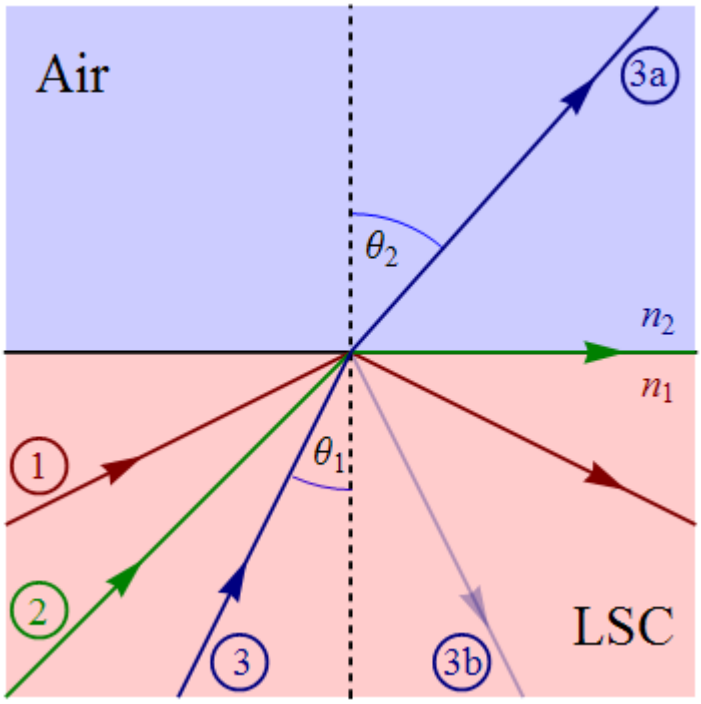

Fig. 2.2.1: A light ray impinging on the LSC-air surface at angles above (1) or below (3) the critical angle (2)

In Fig. 2.2.1 we can see the behaviour of a light ray emitted inside the LSC and impinging on the surface:

1) If the angle of incidence is above the critical angle (that is the angle between the ray and the normal to the surface) total reflection occurs and the ray is reflected back into the LSC with an angle equal to the angle of incidence.

2) At exactly the critical angle the ray is refracted at the interface between LSC and air

3) Below the critical angle two phenomena occurs, part of the light is refracted (3a) and part is reflected (3b) according with the Fresnel equations

The probability for a photon to be trapped inside the LSC by the total internal reflection for a given refractive index is:

$$P_{ir} = \sqrt{1 - \frac{1}{n^2}}$$

where n is the refractive index of the material of the slab.

The use of a medium with high refractive index is anyway detrimental because the increase in light trapping efficiency would be thwarted by the parallel increase in the light reflected by the surface as in Fresnel Equations the reflectance is positively dependent on

the refractive index.

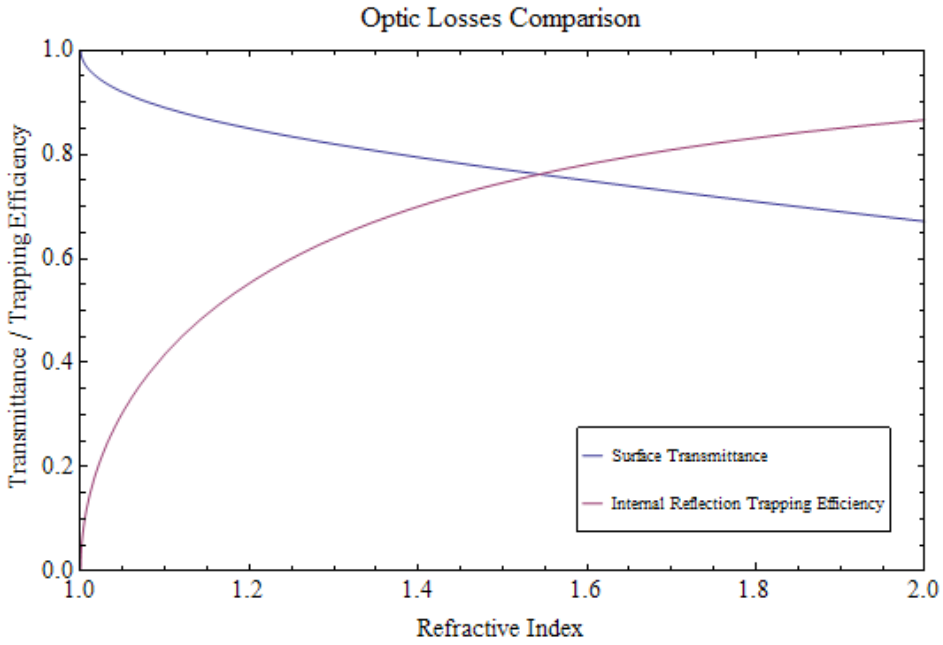

Fig. 2.2.2: Comparison of the escape cone and surface reflectance contributions to the optical losses

Moreover the dye have to be incorporated into the transparent medium so the latter must exist in a liquid phase or be obtained starting from a precursor available in a liquid phase, in this case the typical procedure consists in mixing the dye with a precursor that is later moulded in the desired shape and polymerized stabilizing the dye into a solid matrix.

This procedure is clearly feasible only for plastics and silicones, another technique consist of incorporating the dye into the molten medium but the exposure to high temperatures could decompose the dye (organic and organometallic dyes) or alter its electronic properties (quantum dots).

For all of these reasons LSCs are commonly manufactured employing polymethylmethacrylate (PMMA), polycarbonate (PC) or silicones with high refractive index but these materials are non very hard and are prone to scratching: if a more scratch resistant surface is needed a soft optical medium (such as silicone) could be laminated between two layers of clear glass.

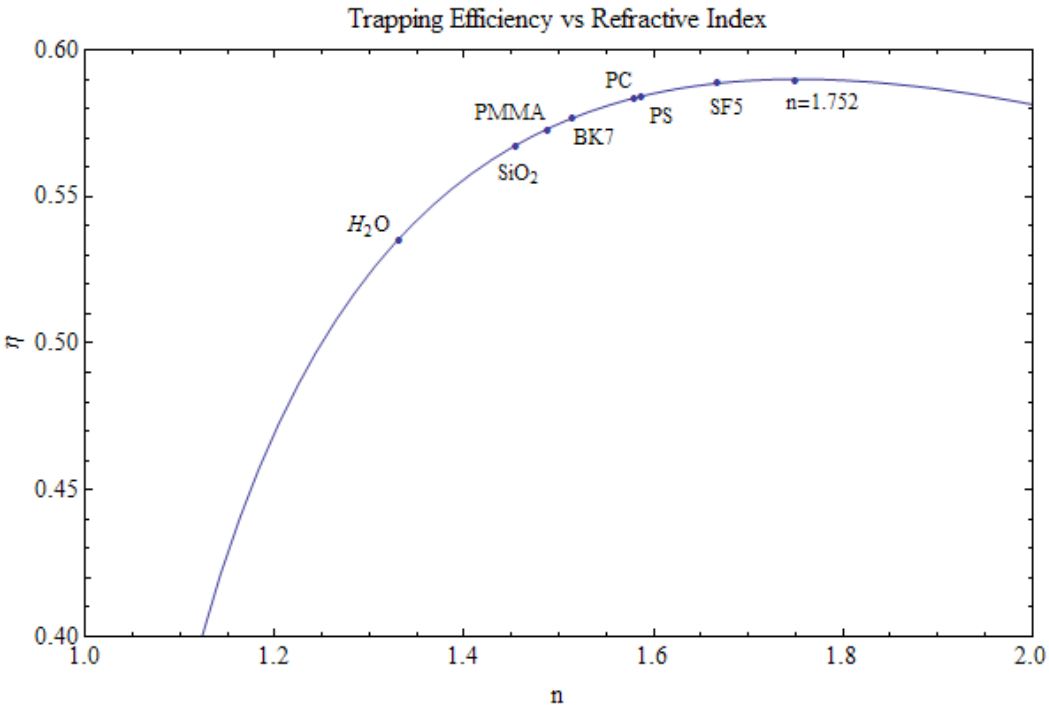

Fig. 2.2.3: Combining the two contributions we get the maximum optical efficiency for a given refractive index, since it is not constant and depends on the wavelength the refractive indexes at 632.8nm (HeNe laser wavelength) were taken. As a reference some common optical materials are shown: water (H_2O), fused silica (SiO_2), polymethylmethacrylate (PMMA), BK7 crown glass, polycarbonate (PC), polystyrene (PS) and SF5 flint glass.

The maximum in the efficiency curve is located at n=1.752: this is a high refractive index achievable only by heavy flint glasses and far from plastics and silicones that rarely exceed 1.6.

The refractive index of PMMA (1.489) however is far from ideal but lies in a region where the efficiency curve is rather flat so the difference from the maximum value (η=0.590) is only 2.97%.

2.3 Overall optical efficiency

Summarising, the overall optical efficiency can be expressed as:

$$\eta_{opt} = T\, P_{ir}\, \eta_{ir}\, \eta_{abs}\, \eta_{qy}\, \eta_{Stokes}\, \eta_{sa}$$

Where:

T is the transmittance of the LSC surface and depends on the refractive index of the transparent medium

P_{ir} is the probability of trapping by total internal reflection and depends on the refractive index of the transparent medium

η_{ir} is the internal reflection efficiency and depends on the flatness of the surface

η_{abs} is the absorption efficiency of the fluorescent dye

η_{qy} is the quantum efficiency of the fluorescent dye

η_{Stokes} is the energy transfer efficiency from the absorbed photon to the emitted one and depends on the Stokes shift of the fluorescent dye

η_{sa} is the probability for an emitted photon of not being re-absorbed by the dye

2.4 Inclusion of reflective surfaces

Luminescent solar concentrators do not rely on curved optical elements to achieve a concentration of the light, it is the light trapping caused by the total internal reflection inside the slab that gives them their light concentrating characteristics.

In an LSC employing an ideal dye without self absorption the concentration would be proportional to the ratio between the area of the surface exposed to the light and the area of the sides: for a given shape of the slab the concentration ratio could be increased by increasing the surface area or reducing the thickness.

However these parameters cannot be changed at will because an increase in the surface area or a reduction of the thickness would make the slabs less rigid until they can bend under their own weight.

A practical solution to increase the concentration factor can be the replacement of some of the solar cells with reflective surfaces, which task is to keep the light inside the LSC until it is absorbed by the solar cells.

Various optical setups were evaluated with, in particular, the concentrators with some cells replaced by mirrors seeming very promising because the addition of mirrors proves useful to even out the profile of irradiance on the cells by redistributing more uniformly the light.

Moreover the introduction of the mirrors reduces the amount of cells needed for a given system power and simplifies the assembly process.

Mirrors however present some drawbacks, the most significant is their non perfect reflectance that leads to absorption losses so the higher is the amount of cells replaced by mirrors the higher are the losses so the optimal balance between the losses caused by the current mismatch and the absorption of the mirrors must be found.

There are two approaches for the placement of the reflective surfaces: they can be placed at the corners of the slab of can replace entirely the solar cells on a side: both solutions were evaluated in the simulations and the ones that proved more effective were chosen to manufacture the prototypes.

3 Numerical simulations

The solar cells placed on the sides of the LSCs are series-connected so any mismatch in the current produced by each cell would result in a significant efficiency loss thus, in order to evaluate how the geometry of the concentrator affects the power production, numerical simulations of light transport inside the LSCs have been carried out.

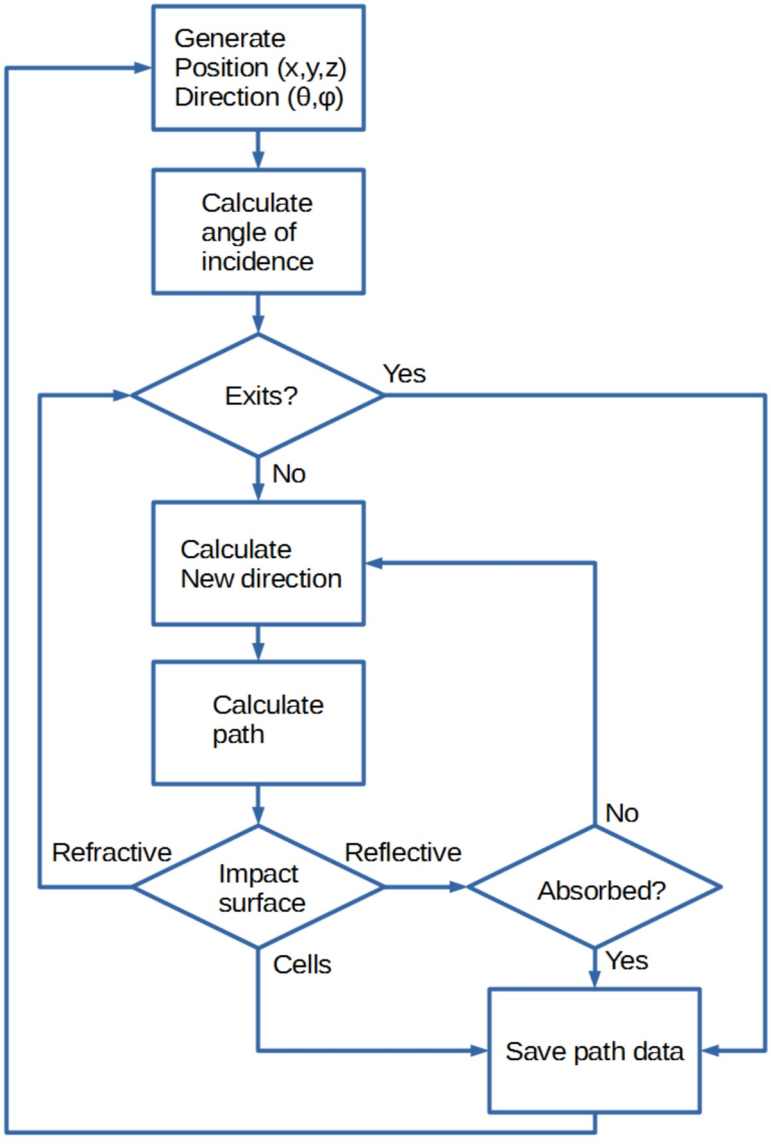

Fig. 3.1: This flowchart represents he algorithm of the raytracing simulation, the data about the path of the photons is later elaborated in order to obtain the profile of irradiance on the surfaces and the expected current production of the cells

The simulation software have been written on purpose for this work using the C programming language and have been optimized to run on multiple-core CPUs, the relative values of the irradiance on the sides of the LSC are obtained with a raytracing technique and the expected short circuit current produced by each cell is obtained integrating the irradiance distribution over the cell length.

The photons are generated inside the LSC with a uniform spatial distribution while the directions have a uniform angular distribution, the path of each photon is a straight line that ends on a surface of the LSC.

Three types of surfaces are considered: refractive, reflective and absorbent.

Refractive surfaces represent the LSC-to-Air interfaces where, depending on the refractive index of the LSC, the photon can undergo total internal reflection or exit from the surface, in the latter case it is considered lost and the exit point is saved in the path data.

The partial reflection at angles close to the critical one is not considered because its contribution to the trapping efficiency is negligible in large area LSCs due to the multiple reflections needed to reach the sides.

The reflective surfaces represent the sides covered with the mirror film, in this case the reflectivity R of the film is considered, when a photon strikes a reflective surfaces a random number with range from 0 to 1 is evaluated and if it is higher than the surface reflectivity the photon is absorbed by the surface. Even if the reflective manufacturer states a reflectivity above 99% in these simulations it is set at 0.95 to account for possible assembly errors.

The absorbent surfaces represent the solar cells which are simulated as perfect absorbers, the following table summarises the parameters of the simulations.

Parameter	*Value*
Flux of photons	$1.6 \cdot 10^8$ photons/m^2
Mirrors reflectivity	R=0.95
Solar cells reflectivity	R=0
LSC refractive index	n=1.489 at 650nm

When a photon is absorbed or lost the software saves its path data which consist of the source point and direction, the points where it was reflected by the surfaces, the outgoing direction after each reflection and the surfaces type.

Analysing these data it is possible to generate the expected irradiance profile on each

surface as well as to evaluate the amount of photons lost due to escape cone losses or absorption by the reflective surfaces.

Various optical setups were evaluated, the reference design consists in a square LSC with solar cells applied on all four sides and without any reflective surface, this have been taken as a reference because it represents the most common LSC design.

The other optical setups simulated consist in square LSCs with solar cells on only one or two sides and with the other sides covered with a mirror film and LSCs with solar cells an all four sides but employing receivers with some of the cells replaced by the reflective film, some exotic setups have also been evaluated as asymmetric designs with some cells replaced by mirrors.

In the following charts a schematic picture of each LSC configuration is provided, the sides in blue represent the solar cells while the grey colour represents the reflective film. Each surface is numbered in order to provide a visual reference for the surfaces shown in the charts.

3.1.1 25cm square – cells on four sides – 10 cells per receiver

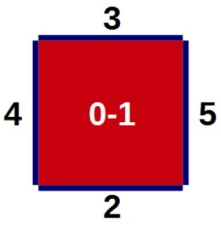

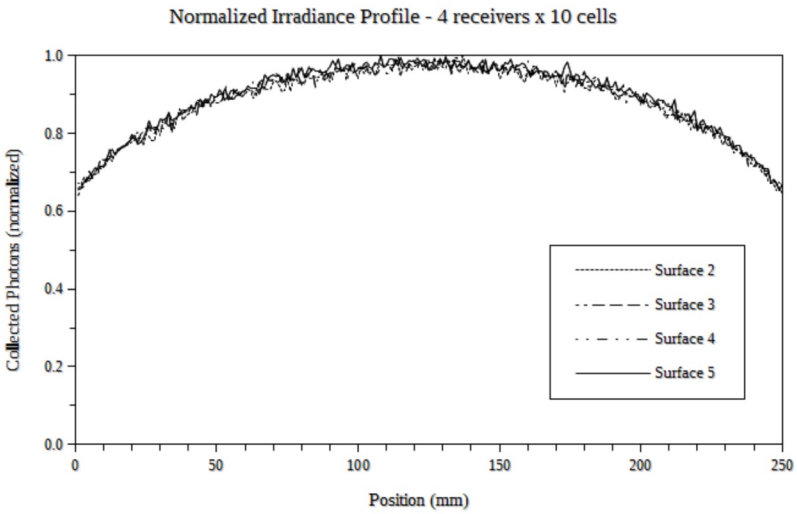

In absence of reflective surfaces the irradiance profile follows a cosine function. In this configuration, having cells on all sides, the absorption is maximum but the uneven irradiance profile doesn't permit to take advantage of this situation unless cells of different sizes are used or cells of equal size are connected in parallel.

Both these approaches would be effective but at the same time impractical in the perspective of an industrialization attempt.

The use of cells of various sizes would make impractical the scaling of the concentrator up to larger areas as this would require the stocking of a large number of components (the cells) which all serve the same purpose, moreover, in order to fit correctly the different irradiance levels across the same side, the larger cells should be 50% larger of the smallest ones.

The cells used in LSC fabrication are strips a few millimetres higher than the concentrator thickness, for this reason the longer cells become extremely fragile and the maximum size that can be handled by the assembling machines is limited. If the largest cell size is limited an approach with cells of different sizes obviously requires the use of more cells to cover the same length.

Connecting all the cells in parallel would be equally infeasible as it would result in an output with a high current and low voltage which requires the use of large conductors and leads to significant losses in dc-dc and dc-ac conversion.

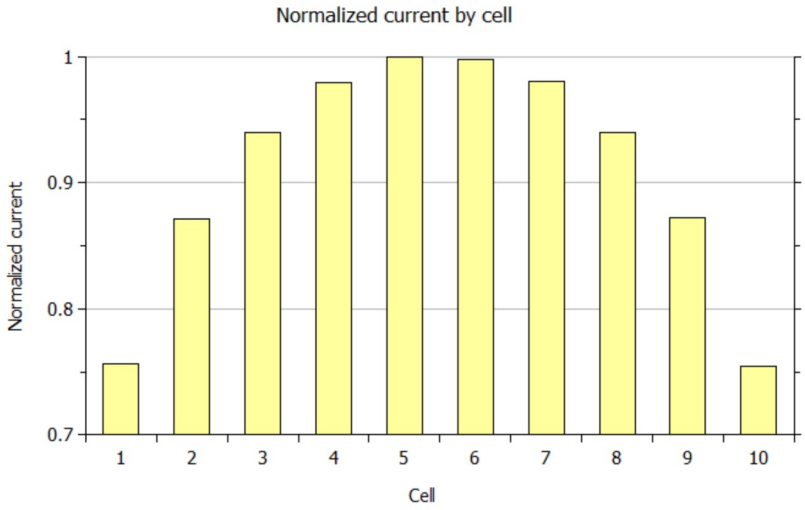

With this configuration if a cell length of 25mm is considered, the mismatch in current production between the central cells and the ones at the ends of the same receiver would be approximately 33%.

Such a situation is far from ideal but represents a reference to evaluate the effectiveness of the other configurations.

3.1.2 25cm square – cells on two sides – 10 cells per receiver

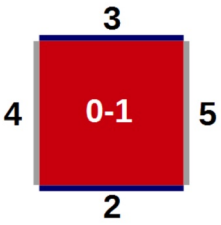

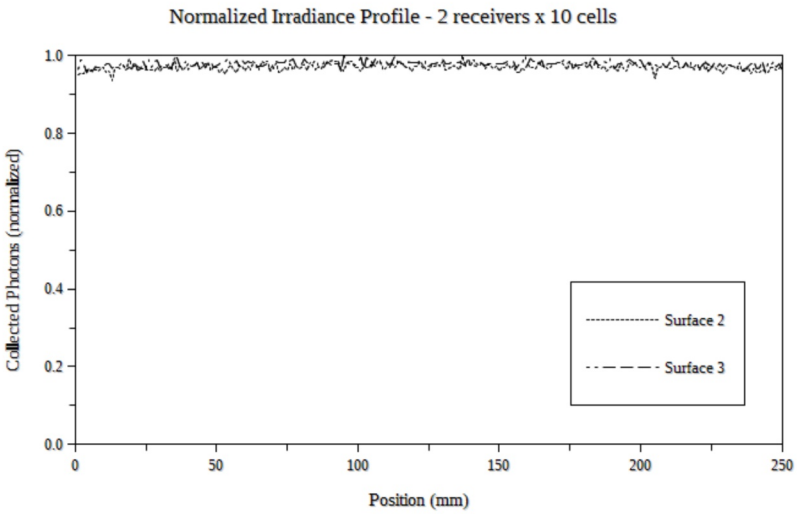

Removing two receivers and replacing them with reflective films have a dramatic effect on the irradiance profile because the huge difference (approximately 50%) in irradiance between the centre and the ends seen in the reference design in this case becomes less than 3%.

This close-to-ideal irradiance profile comes at the cost of absorption caused by the reflective surfaces whose reflectivity have been estimated around 95%, this means that photons undergoing multiple reflections on the sides are likely to be lost due to absorption by the reflective film.

This effect is anyway less significant than the current mismatch seen in the reference configuration and results in a higher efficiency.

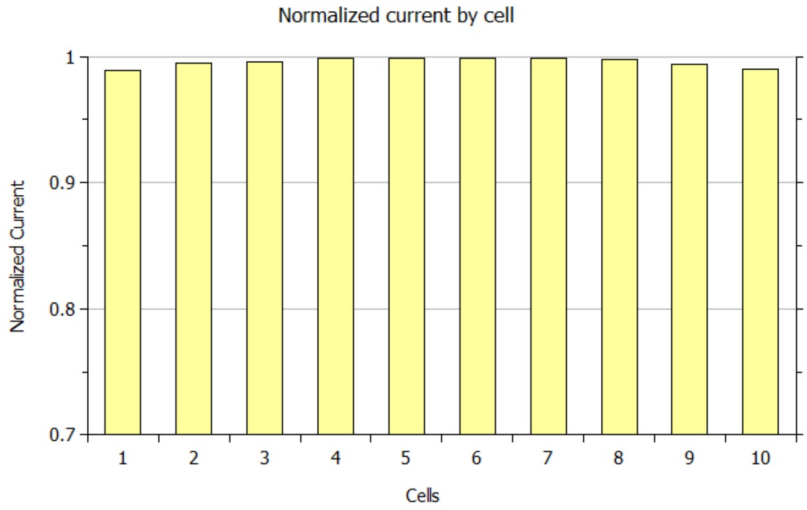

The current mismatch among the cells is minimal, this small variation in current production will be probably less noticeable than the statistical variation between the cells and the effect of small assembly defects.

3.1.3 25cm square – cells on one side – 10 cells per receiver

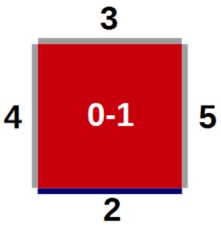

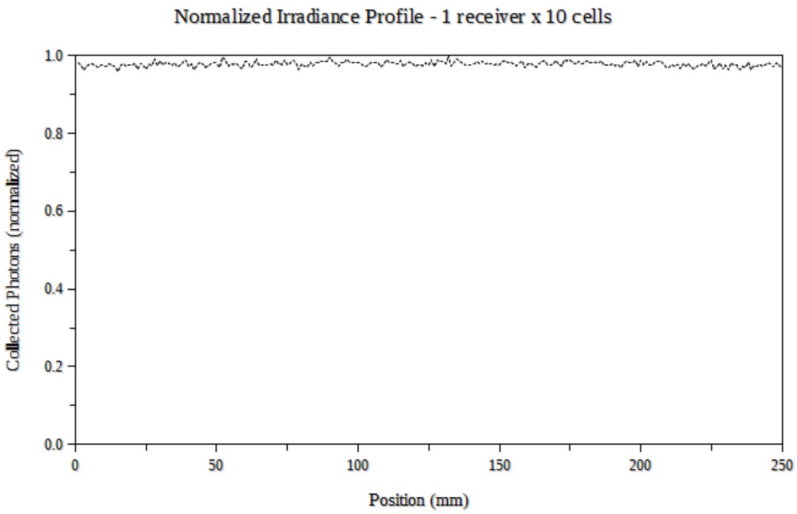

With three sides covered by a reflective film there is no noticeable improvement in the flatness of the irradiance profile but at cost of a higher absorption that makes this design less efficient than the previous.

This design anyway requires only a fourth of the cells employed in the reference design and hence represents the most affordable if we take into consideration the price-to-efficiency ratio.

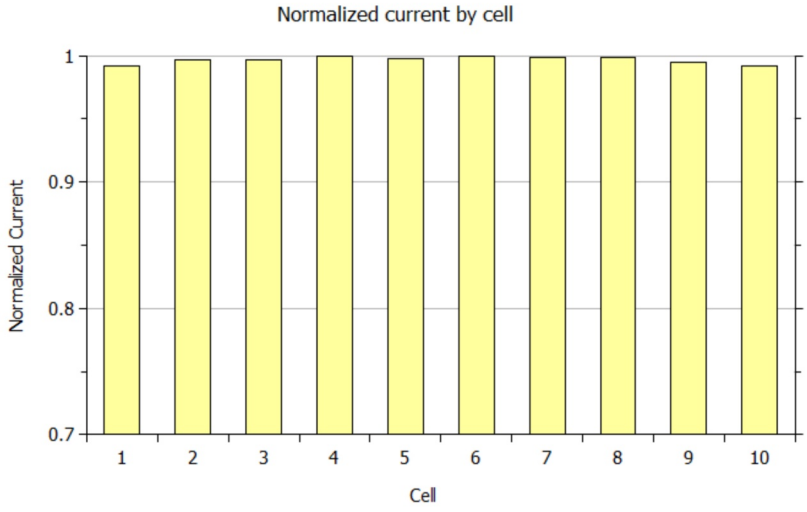

3.1.4 25cm square – cells on four sides – 8 cells per receiver

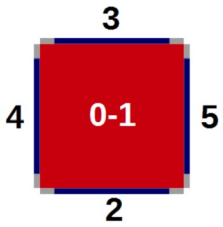

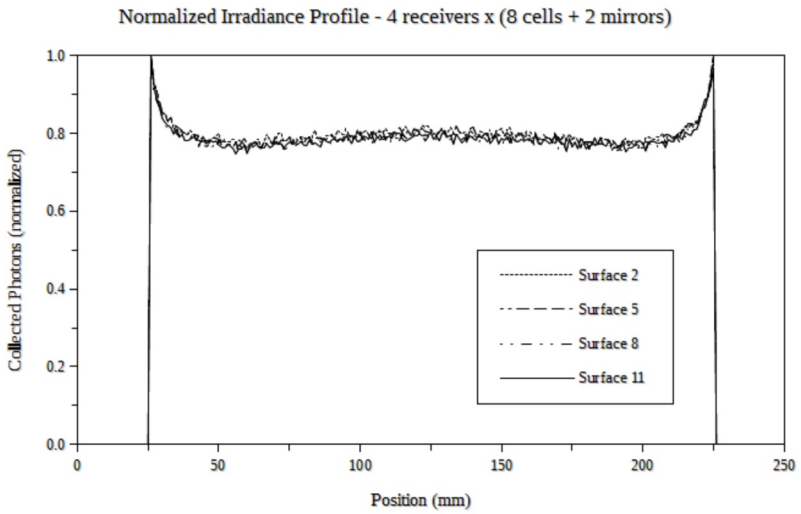

Covering only the corners of the LSC, which represent the areas with lowest irradiance, seemed a good idea but the resulting irradiance profile presents a couple of problems.

The first problem is the presence of sharp peaks at the cells to mirror junction that make it extremely sensitive to assembly errors because any error would result in a significant current loss.

The second one is the current mismatch among the cells that, albeit limited to 6%, is worse than in the previous configurations.

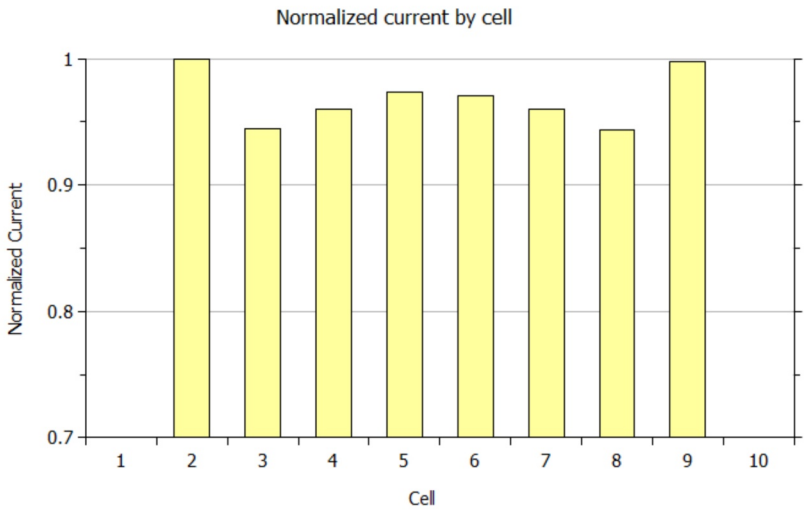

3.1.5 25cm square – cells on four sides – 9 cells per receiver

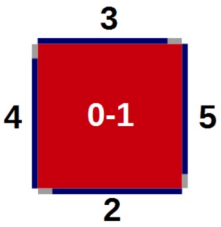

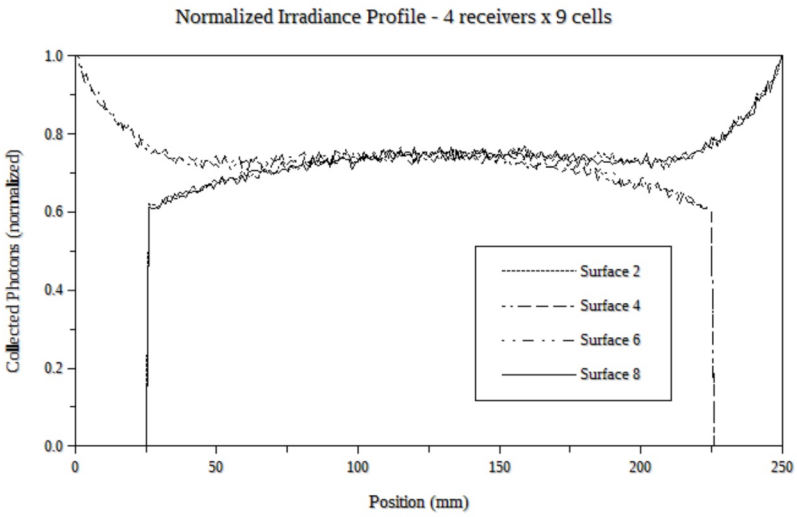

This strange configuration have been tested mainly to see how the software dealt with asymmetrical configurations: in this case the software performed flawlessly but the irradiance profile shows the highest variations among the evaluated configurations, even worse than the reference, and is therefore almost useless.

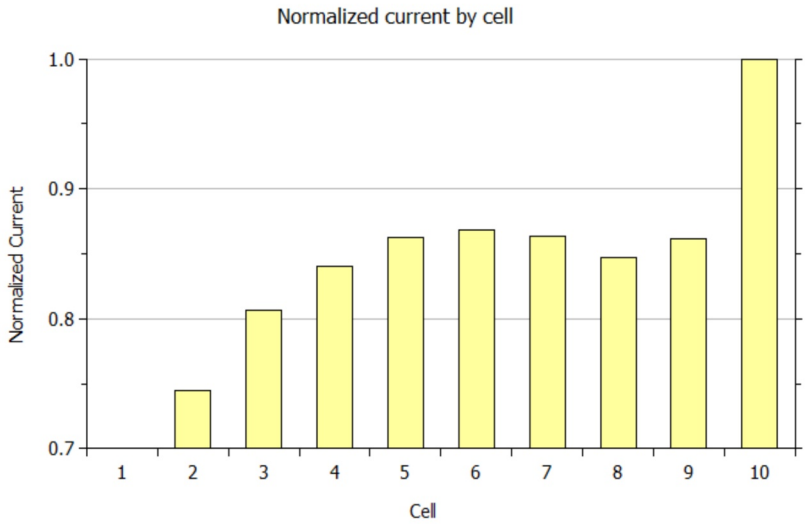

3.1.6 25cm square – cells on two sides – 8 cells per receiver

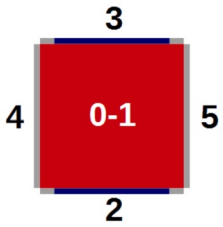

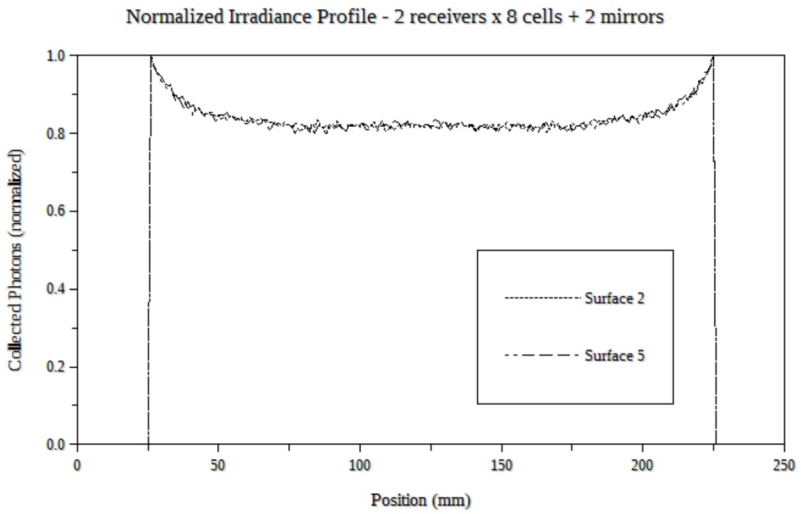

Looking at the good performance of the configuration with two reflective sides this configuration with two receivers with eight cells each seemed to be promising but the result turned out to be very disappointing.

The reflective sides help to even out the irradiance profile but this process results in a higher current mismatch between the cells, the widening of the peak at the cells-to-mirror junction causes an increase in the current produced by the extreme cells which results in an increased mismatch between the cells.

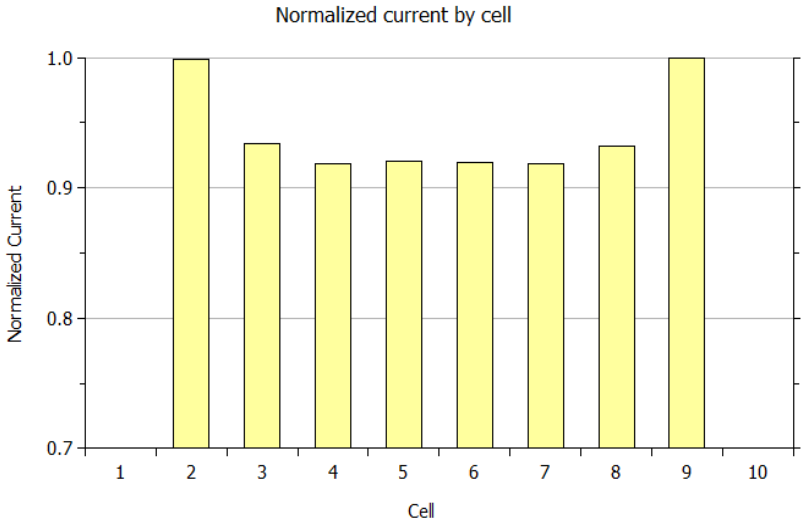

3.1.7 Summary

Among the various setups evaluated in these simulations only three seem to be worth further investigation: the reference design with cells on all four sides, the design with cells on two sides and the design with cells on one side only.

The best theoretical performance is achieved by the configuration with two reflective sides that balances the good uniformity in the irradiance profile with reduced losses caused by multiple reflections on the mirrors.

The setup with the cells placed only on one side of the slab have an irradiance profile similar to the system with the cells on two sides but with a lower power output caused by the increased number of reflections on the sides and therefore the increased chances of absorption.

Anyway this configuration is interesting from an economical point of view because is the one using fewer cells that are the most expensive component in LSC systems.

3.2 Impact of shading

All solar panels suffer a significant loss in efficiency when subject to partial shading but flat panes installed on the roofs or in well designed power plants are unlikely to experience this problem. In high power systems a partial shading could even result in a permanent damage of the cells if bypass diodes are non properly installed.

Solar panels designed for building integration, instead, are likely to be subject to shading caused by nearby buildings, trees or architectural features of the building.

A design tolerant to shading is therefore advisable so the behaviour of the most interesting designs previously identified (with cells on four, two and one side) were simulated under significant shading patterns.

In the following graphs in addition to the irradiance profiles on the receivers are present are shown also the photons lost from the escape cone and the photons absorbed by the reflective surfaces.

Moreover, in the schematic picture of the LSC, the shaded area considered in the simulation is filled with a darker colour to give a visual reference to the reader.

3.2.1 25cm square – cells on four sides

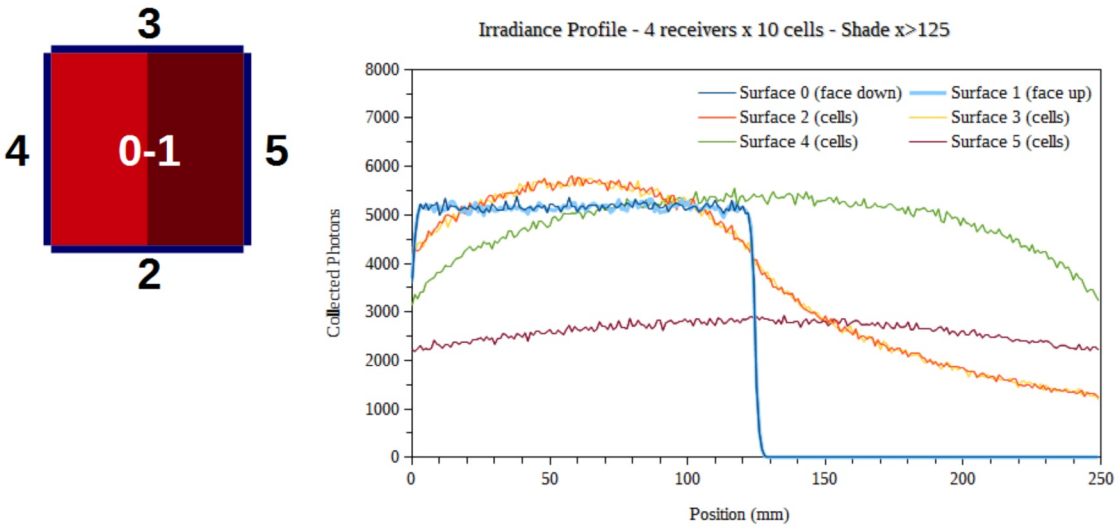

Being symmetrical on two axis, only one shading pattern has been simulated for this configuration.

The irradiance peak on sides 4 and 5 corresponds to the centre of the side while for the half-shaded sides 2 and 3 corresponds to the centre of the illuminated zone.

The chart shows that the half-shaded receivers receive the same irradiance profile (given that the system is symmetrical) which presents very large variations ranging from the highest irradiance value to the lowest. This would result in a strong current mismatch and a consequent loss in efficiency of the system.

The side completely unshaded side presents an irradiance profile identical to the unshaded condition.

Surprisingly the lowest and highest irradiance values are located on the half-shaded sides while the completely shaded side shows a relatively uniform irradiance profile therefore do not represent the limiting factor for the system power output.

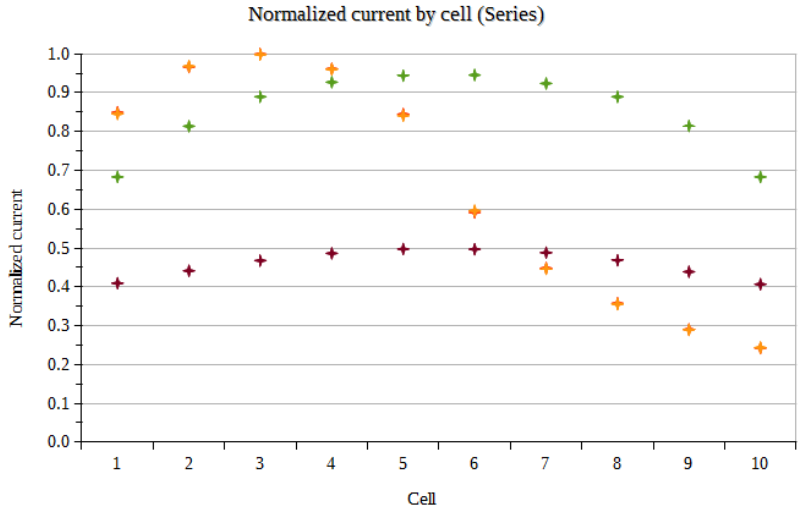

As expected, looking at the irradiance profiles the current produced by each cell shows the highest value for cell 3 of the half-shaded receivers and the lowest values in cell 10 again of the half-shaded receivers.

With this configuration the best cells are producing four times the current of the worst cells leading to a dramatic power loss.

3.2.2 25cm square – cells on two sides

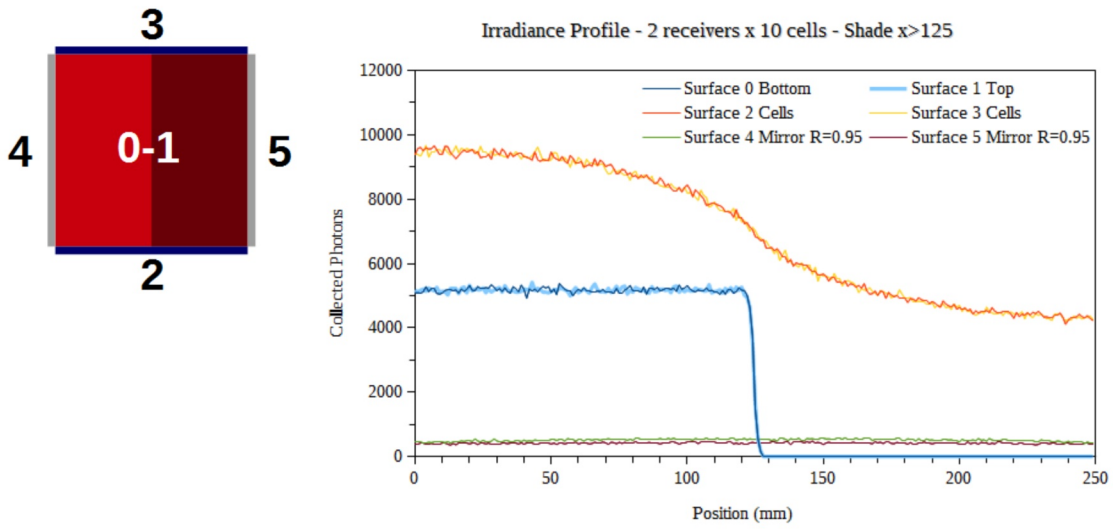

When two receivers are replaced by mirrors, the mismatch seen before is effectively mitigated, the irradiance peak is located at the illuminated end of the receivers and the difference between the maximum and minimum values is 2.4x.

With a reflectivity of 0.95 the absorption caused by the reflective surfaces is negligible and its effect becomes acceptable if the increased flatness of the irradiance profile is considered.

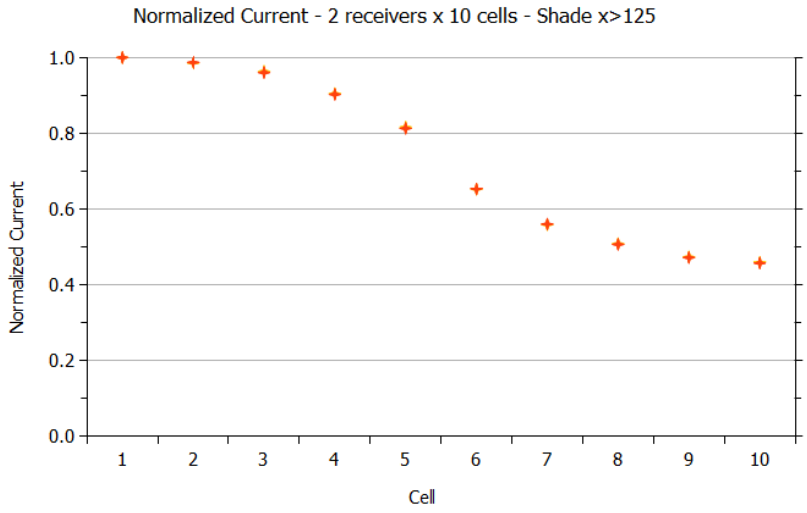

Looking at the expected current production of the cells is evident the reduction in the mismatch, in the configuration with four receivers the best cells produce a current four times higher than the worst but in this case the difference is reduced to 2.4 times leading to a significant improvement in system efficiency.

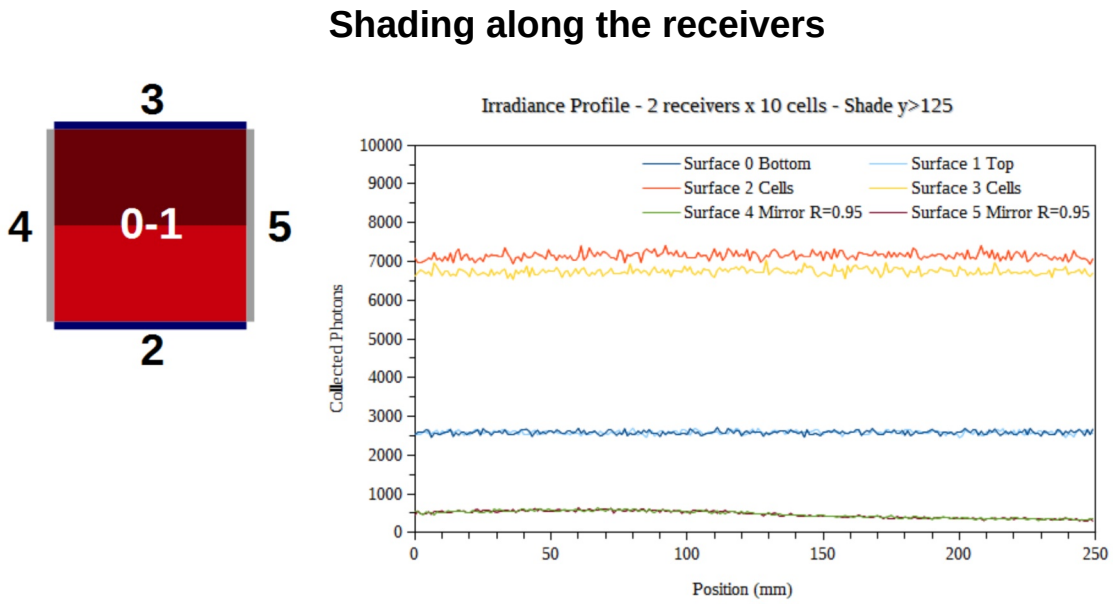

Shading along the receivers doesn't seem to affect significantly the performance of this system, a difference in irradiance between the two sides is anyway present but is not as dramatic as with the shading across the receivers.

The single irradiance profiles, on the two surfaces hosting the cells, show the same difference of 3% between the highest and lowest values previously seen without the shading.

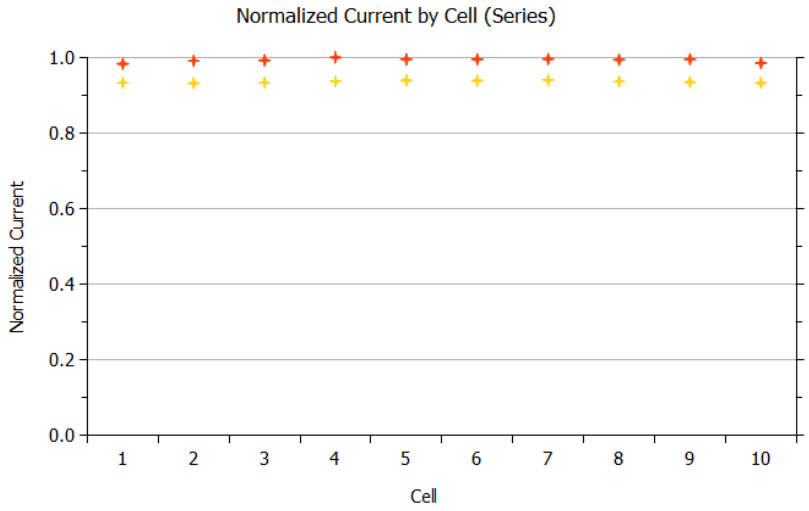

In this case the mismatch between the receivers is reduced to 10%, a good result that permits to this system to perform well, even if partially shaded, with a reduced efficiency loss.

3.2.3 25cm square – cells on one side

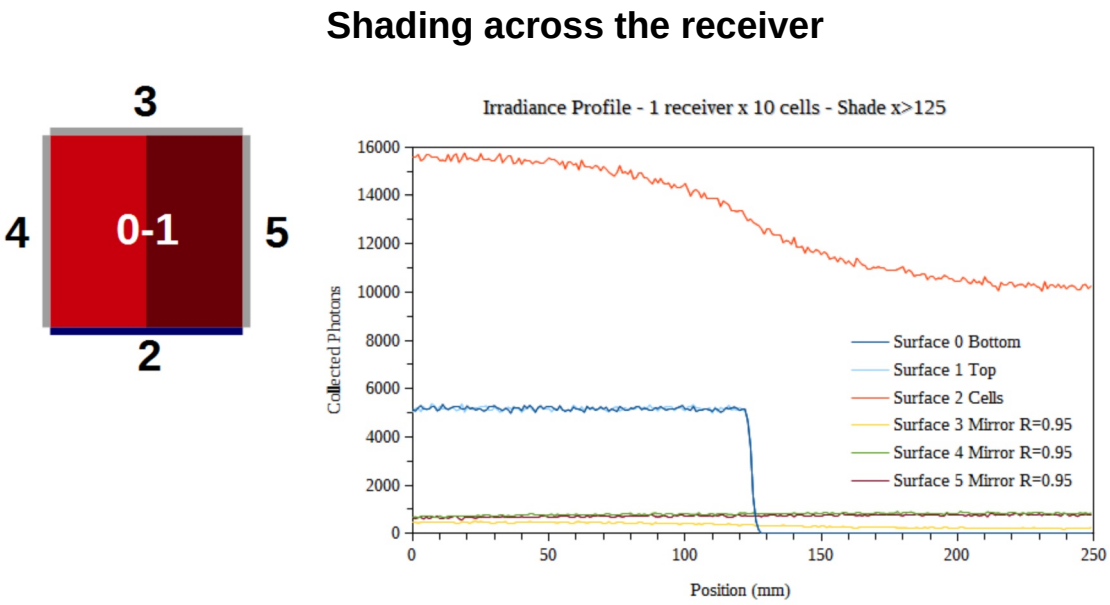

The addition of a third reflective surface results in a further flattening of the irradiance profile, in this case the difference between the highest and lowest irradiance values is limited to 50%: a remarkable result for such an extreme shading pattern.

As expected looking at the irradiance profile, the mismatch among the cells is the lowest seen so far for this shading pattern with the best cells producing 1.5 times the current of the worst cells.

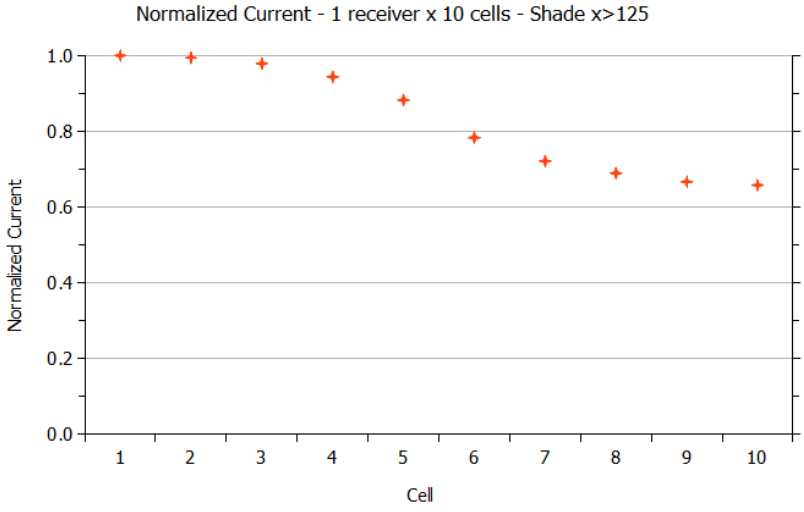

Shading along the receiver – mirror side

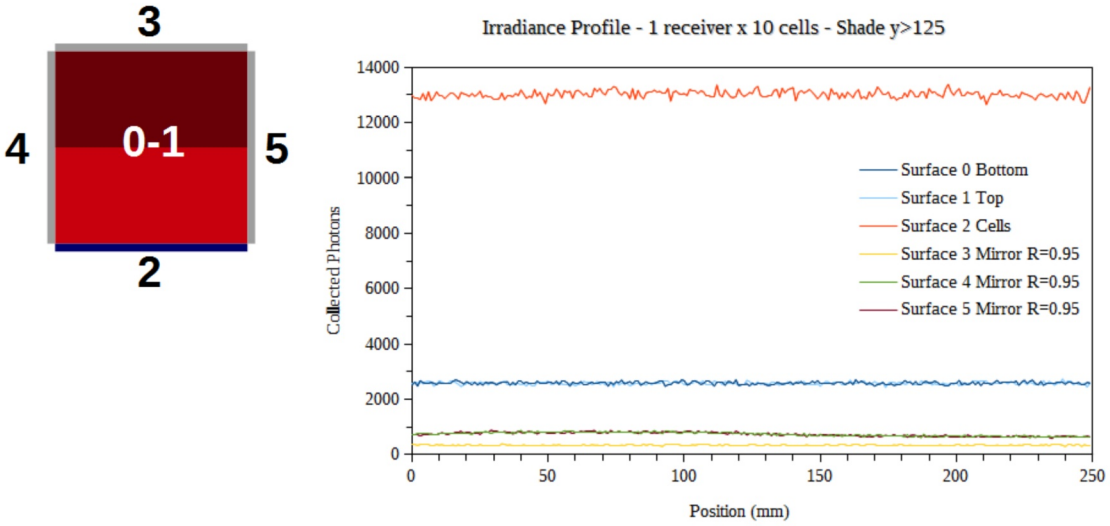

Shading the half of the LSC not comprising the receiver has a little effect on this configuration: the irradiance profile is as flat as without shading.

The current mismatch among the cells is negligible, therefore with this shading pattern the system shows no efficiency loss.

The graph showing the expected cell current is missing because, being a straight line, it would be hardly significant.

Shading along the receiver – cells side

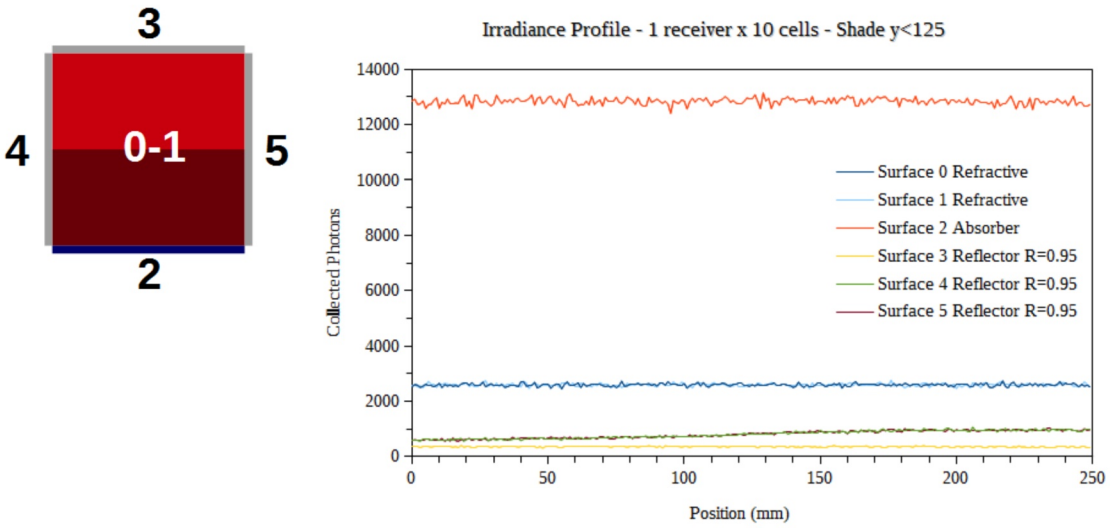

As in the previous case the irradiance profile is flat and the current produced by the cells

is matched.

Looking at all the shading patterns this system performs better than the other configurations under partial shading and, adding the reduced cost and ease of assembly and wiring, is clearly the best candidate for industrialization.

Again, the graph showing the expected cell current is missing because, being a straight line, it would be hardly significant.

3.2.4 Summary

While the simulations considering a uniform exposure of the panels pointed at the system with cells on two sides as the best performing configuration, in these simulations considering different shading patterns the clear winner is the system with only one receiver.

Under all the shading patterns evaluated this system have shown the lowest current mismatch among the cells

This is a remarkable result because the simulations showed that the system employing less solar cells, and thus being the cheaper and easier to manufacture, if properly designed performs better, under all the aspects, than more complex and expensive designs.

Obviously these results should be confirmed by the tests on the prototypes but the results of the simulations are very encouraging.

The next two chapters will cover the assembly process of the prototypes and their performances with the same shading patterns studied in these simulations in order to asses how reliable they are.

4 Assembly process

The modules consist of square slabs of PMMA doped with a concentration of 300ppm organic dye belonging to the commercial Lumogen family, the slabs are 5mm thick and are laser cut to a size of 25×25cm and 50×50cm.

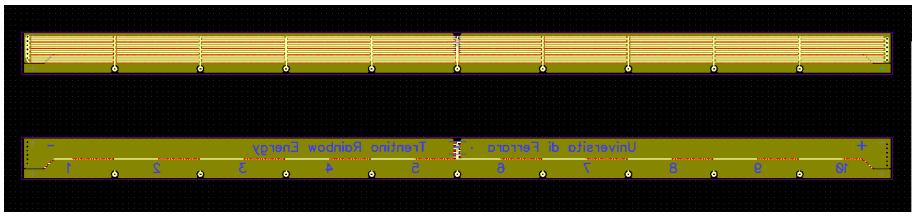

Fig. 4.1: The printed circuit boards of the receivers were purposely designed for these luminescent solar concentrators

The LSC slabs are coupled with monocrystalline back-junction back-contact silicon solar cells cut to a size of 23×8mm, these cells are arranged in arrays of 10 cells connected in series and soldered onto a printed circuit board (PCB).

These PCBs, which have been developed within this work, provide all the necessary electrical connections and act as heatsinks. The PCB have also test points that allow to perform measures on each cell of the array.

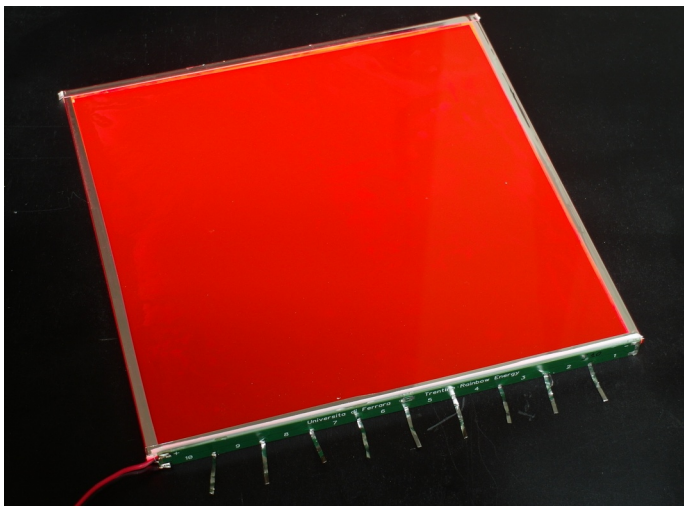

Fig. 4.2: A prototype using one receiver showing the contacts used to test individually the cells of the array

The PCB with the cells soldered on is called receiver and acts as the base module used to assemble the systems, each system employs one or more receivers depending on the length of the sides and the optical configuration.

All the PCBs were fully tested after assembly, performing an IV curve of the array and of the individual cells, in order to remove the defective ones and assure the absence of defects in the prototypes.

The modules were assembled mounting the receivers on the edges of the slabs using an optical UV glue, the surface of the LSC close to the cells have been protected from the glue by a strip of reflective mirror 5mm wide, otherwise an excess of glue may have directed part of the light to the PCB instead than on the cells.

The sides without cells were covered with a high quality reflective film based on dielectric layers whose characteristics are described in detail in 4.4.

4.1 Cells cutting technology

The cells used to manufacture the systems were cut from commercial back-junction back-contact solar cells, each wafer is 156×156mm with chamfered edges and yields 56 (14×4) sub-cells with a size of 23×8mm.

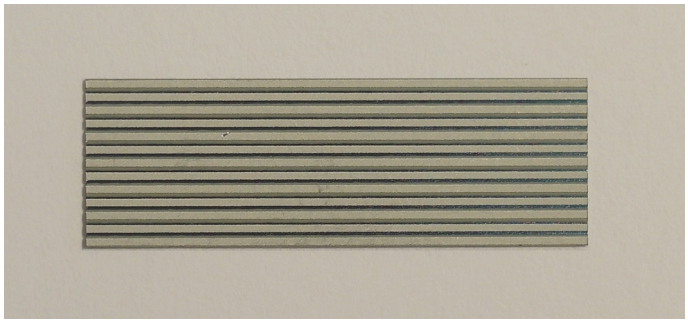

Fig. 4.1.1: Picture of the back side of a cell, the contacts are the white horizontal stripes. There are 13 contacts so the first and last one have the same polarity (cathodes) in order to avoid assembly errors

The cells are cut to a size that permits to have two cathode contacts close to the edges, in this way there is no need to care about the orientation of the cell: an expedient that greatly simplifies the assembly process.

Two cutting techniques were evaluated: the first cells were cut mechanically using a dicing machine with a diamond blade.

Later, in order to build more quickly more prototypes, the cells were laser-cut by the Applied Research Institute for Prospective Technologies of Vilnius (LT)

Batch	*Cutting quantity (front side)*	*Laser Power*	*Cutting quantity (back side)*	*Laser Power*
1.	2 times	100%	0 times	0
2.	2 times	100%	0 times	0
3.	2 times	80%	1 time	50
4.	2 times	80%	0 times	0
5.	2 times	60%	0 times	0
6.	1 time	100%	0 times	0

Some laser cutting recipes were evaluated in order to find the one less damaging to the cells, since the solar cells were back-junction back-contact most cuts were performed on the front in order to cause the least damage to the junction.

At least 20 good cells cut with the laser using each recipe as well as with the dicing machine were soldered on the receivers and individually tested, both the power produced by the cells and the fill-factor were measured.

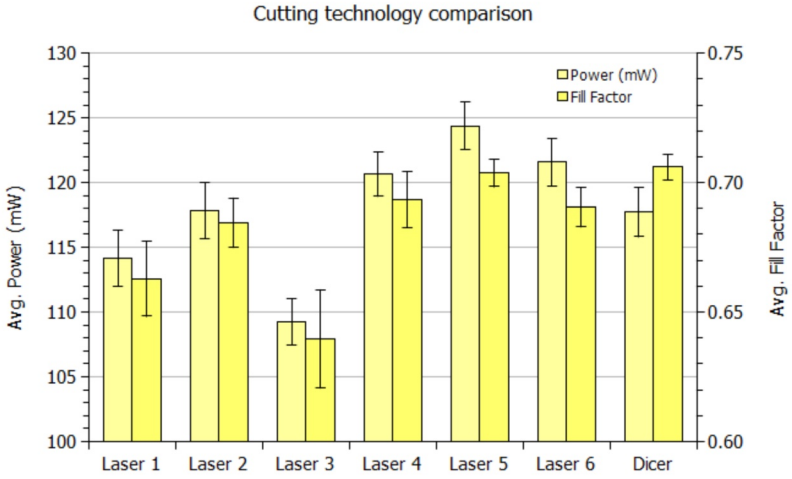

Fig. 4.1.2: Performance of the cells cut using various techniques

Recipe 5 was chosen due to the best power production and the fill-factor comparable with the cells cut using the dicing-machine.

4.2 Glue selection

Two types of glue were evaluated: a two components acrylic glue purposely sold to glue PMMA and an optical UV curing glue with an index of refraction close to PMMA and that exhibits a good adhesivity to PMMA.

The first glue tested was Anglosol 700 [10], a two part acrylic adhesive that consist in a monomer (MethylMethAcrylate – MMA) based component (Component A) and a peroxyde catalyst (Component B) that must be mixed with a ratio 20:1 of monomer to catalyst.

Setting occurs by polymerization of MMA into PMMA that is the same material of the slabs so bonding is perfect as long as the surface have been cleaned thoroughly, bonding to other surfaces is generally good but must be verified.

In particular the strength of the bonding to fibreglass and silicon solar cells have been tested, fibreglass is bonded poorly while the solar cells are strongly bound by the adhesive probably due to the textured surface that increases the contact area.

Being based on the same material as the slabs the adhesive has also the same refractive index and therefore the optical coupling in case of a good joint is perfect.

The main drawback of this adhesive are the poor weathering properties, in particular after prolonged outdoor exposure the glue can exhibit some yellowing and embrittlement, another problem is the long hardening time that turns the assembly into a very slow process because the joint can be handled only after at least 1,2-2 hours while the maximum strength is reached after 24 hours.

A faster setting compound is the Delo Photobond GB368 [11] that is a one-component UV-curing adhesive specifically formulated to glue optical devices made of glass, plastic or metal.

This glue has a refractive index of 1.506, slightly higher than PMMA (1.489) but close enough to achieve a good optical coupling between the slab and the cells.

This adhesive sets quickly upon exposure to ultraviolet light in the range from 320 to 420nm, the exact setting time depends on various factors as wavelength, irradiance, and thickness of the glue layer but is in the order of tens of seconds. The manufacturer gives a minimum setting time of 15s when exposed to an irradiance of $60mW/m^2$ by a LED with a wavelength of 365nm.

The main advantage of this adhesive is precisely its fast setting time that eases the assembly process, moreover it maintains a good transparency and resilience even after a long weathering.

We found no significant difference in the performances of cells glued with these two adhesives so, given the better working and mechanical characteristics, the UV glue was chosen and polimerization was performed by mean of an array of five GaN UV LEDs.

These LEDs have an emission peak of 365nm and a peak radiant flux of 1000mW at 700mA and are mounted on an aluminium profile acting as a heatsink with a spacing of 50mm.

4.3 Bending of receivers

The receivers are printed circuit boards with the solar cells soldered on, the back side of the board hosts the electric contacts needed to test individually the cells and to connect the receivers to each other in series or in parallel.

In the process of soldering the receivers develop a strong bend caused by the different coefficients of thermal expansion of the materials that they are made of because the main component of the PCB is FR4: a type of fibreglass commonly used in circuit boards that has a thermal expansion five times higher than silicon.

Material	**Linear thermal expansion coefficient ($10^{-5}\,K^{-1}$)**
Aluminium	2.3
Copper	1.7
FR4 (polymer reinforced fibreglass)	1.2÷1.4
Silicon	0.26

In some cases the far ends of the receivers were not properly glued because the resilience of fibreglass pulled them away from the LSC slab.

A possible solution has been identified in the use of thinner PCBs (from 1.5 to 0.5mm) with a thicker copper layer, even if copper and FR4 undergo similar thermal expansion copper is plastic while fibreglass is elastic, this means that thinner boards with less fibreglass and more copper can be easily straightened up.

4.4 Reflective layer

Mirrors can be divided in two categories, the most common is represented by mirrors made by exploiting the bulk properties of naturally reflective materials, typically

represented by metals such as aluminium or silver and their properties are necessarily bonded to the material they are made of.

Dielectric mirrors attain their high reflectivity exploiting the constructive interference in the light reflected by multiple layers of materials with alternating high and low refractive indexes, in this way is possible not only to obtain a reflectivity higher than most bulk materials but also to tune the reflection spectrum of the mirror.

Typical materials used in the layers with low refractive index are magnesium fluoride MgF_2 (n=1.37) and silicon dioxide SiO_2 (n=1.54) while the layers with high refractive index are made of tantalum pentoxide Ta_2O_5 (n=2.28), zinc sulphide ZnS (n=2.32) or titanium dioxide TiO_2 (n=2.4).

The reflective layer used to cover the sides without the cells is a high efficiency dielectric mirror film, the DF2000MA manufactured by 3M. This film consist in a dielectric mirror deposited on a plastic film the on the opposite side has a contact adhesive applied: the overall thickness of the film mirror is 104µm.

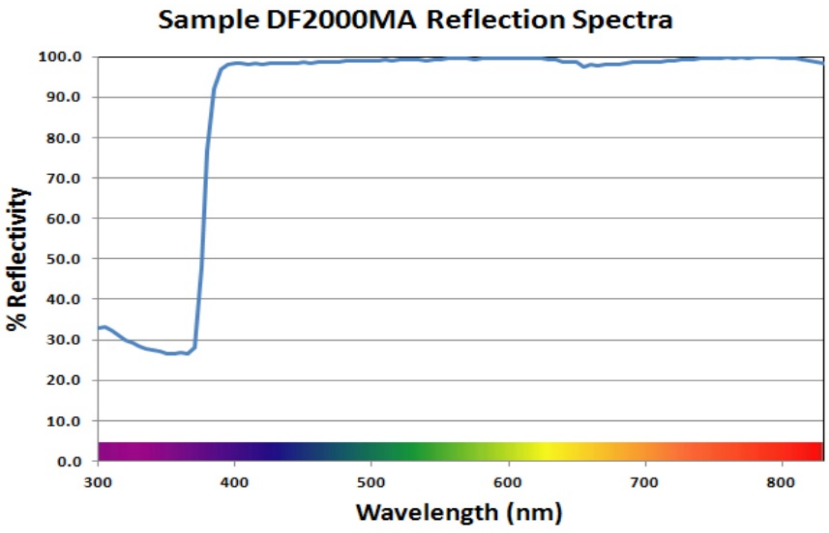

Fig. 4.4.1: Reflection spectrum of DF2000MA mirror film (Source: 3M [12])

The main feature of this film is its high specular reflectivity: higher than 90% in the 400 to 775nm range at an angle of incidence between 0 and 80° that helps to minimize the absorption losses even in case of multiple reflections.

Moreover the adhesive is already present on the film surface so the assembly process is faster but the long-term stability of this layer under UV exposure and high-low temperature

cycles must be further evaluated.

The reflectivity depends on the thickness of the dielectric layers that compose the mirror but on the edges of the slabs the film must accomplish a right angle: the reflective properties of the mirror in those edges must be further evaluated because could represent a significant contribution to the overall light losses.

5 Experimental measurements

5.1 Self-Absorption characterization

In order to evaluate the influence of self-absorption an analysis of the output spectrum of the LSCs have been performed: the slabs were illuminated only on one circular spot at a variable distance from the sides and the outcoming spectrum was measured by a spectrometer so informations about the spectral distribution and global intensity were collected.

The results are shown in the chart, only 4 dyes were tested because the violet dyed performed too poorly

Self absorption is very strong and only the photons outside the absorption spectrum have a diffusion length above 5cm

Yellow and Red dyes exhibit the most significant self-absorption that in the case of Red is balanced by the stronger emission

5.1.1 The Czerny–Turner Spectrometer

A spectrometer is a device whose purpose is to separate a beam of light into its spectral components and measure their intensities, typically, the light intensity is measured by a photodiode or an array of photodiodes like a charge Coupled Device (CCD), digitised by an ADC and sent to a computer where a software displays the data and allows for their further elaboration.

The light beam enters the spectrometer from an input optic system whose output divergence must be known (typically an optic fibre) and passes through a slit that reduces the beam width thus increasing the resolution of the instrument (the narrow is the slit the higher is the optical resolution and the lower is the sensitivity, vice versa for a wider slit).

Later, the beam, which width and divergence are now known, is collimated by a concave mirror that directs the beam towards a diffraction grating that separates the beam into its spectral components according to the law of diffraction

$$\sin(\theta_{out}) = \frac{m\lambda}{d} + \sin(\theta_{in})$$

where θ_{out} and θ_{in} are the angles of the refracted and incident beams, m is the order of diffraction, d is the pitch of the grating and λ is the wavelength.

Later, the beam dispersed by the grating is collected by a second mirror and focused on

the detector, the introduction of the second mirror is particularly useful to permit a practical arrangement of the detector and, extending the optical path, a reduction of the stray light.

The detector is composed by a CCD array of photodiodes, the electronics required to read the signal and a lens to focus the beam on the array: the lens is the only refractive device of the spectrometer and must be manufactured in a material without significant absorbance in the analysed spectrum (Es. fused silica is transparent in the UV-VIS-NIR spectra).

Further details about the spectrometer specifically used for this experiment can be found in Appendix B.

5.1.2 Experimental setup

These measurements were carried out using an experimental apparatus built on purpose that consist in a bench housing the LSC slab and a sled that covers completely the bench, on the sled is made a circular aperture with a diameter of 10mm that permits to illuminate only this spot of the LSC.

The sled is twice as long as the bench, in this way the circular aperture, that is positioned at the centre of the sled, can be moved up to the extreme edges of the LSC while keeping the whole slab shaded.

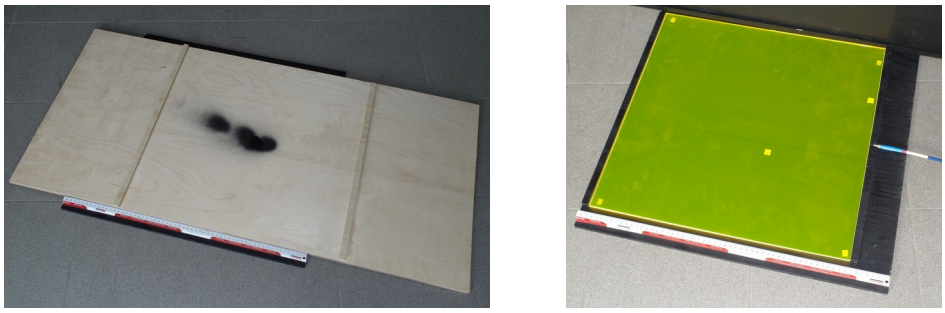

Fig. 5.1.1: The experimental apparatus used to measure the output spectrum of the LSC have been designed and manufactured on purpose for this work

Both the sled and the bench as well as the aperture borders are lined with black velvet in order to reduce the stray light, as a test two measures were taken with the spectrometer: one using the apparatus with the circular aperture closed and one with the input port of the spectrometer closed by a plug and no noticeable difference was present.

The spectrometer is connected through a fused silica optic fibre whose SMA connector on the other side is attached to the bench and is positioned in front of the edge of the slab,

on the same axis as the aperture.

With this setup, as long as the circular aperture is kept in front of the optic fibre input, the optic fibre collects only the light generated by the fluorescent dye in the volume of LSC lit through the aperture, a geometric correction is required to account for the average path length of the photons and the geometry of the aperture.

These corrections are further discussed in the next chapter.

5.1.3 Geometric correction

Let we have a 2D surface and a point source emitting light isotropically, if we add a detector with finite length and whose middle point lies on the same coordinate as the source point the power received by the detector will be proportional to the angle γ subtended by the detector divided by the full circle centred at the source point.

$$\gamma = 2\arctan\left(\frac{l}{2d}\right)$$

where l is the width of the detector and d is the distance between the source point and the detector. So the detector will receive a power

$$I = I_0 \frac{\gamma}{2\pi}$$

where I_0 is the total power emitted from the source.

If the source power is not known, a relation can be found with respect to a measure performed at a distance d_0 taken as a reference

$$I = I_0 \frac{\gamma}{\gamma_0} = \frac{\arctan\left(\frac{l}{2d}\right)}{\arctan\left(\frac{l}{2d_0}\right)}$$

in this case I_0 and γ_0 are the power measured and the angle subtended by the detector at the distance d_0.

Being a device with a surface numerically much bigger than the thickness, a large LSC can be studied as a 2D device whose thickness is considered as a correction factor for the experimental results, therefore the measures taken with the aforementioned (5.1.2) apparatus need to be corrected to account for the shape of the aperture, which has a finite size and is not an adimensional point, represented by factor M and the thickness of the LSC (D).

The expression for the correction factor M is

$$M = \frac{A^*}{A} = \frac{2\int_0^R dr \int_0^\pi d\theta r \sqrt{1-\frac{r^2\sin^2(\theta)}{D^2+r^2-2Dr\cos(\theta)}}}{\int_0^R dr \int_0^\pi d\theta r}$$

And can't be solved analytically so the correction factors for the experimental measures were calculated numerically, further details about how this expression is obtained are available in Appendix C Circular Spot and Distance Correction.

The thickness of LSC influences the average path length of the photons collected by the optic fibre with the minimum path possible being a straight line from the emission point to the detector. The longest possible path is travelled by a photon emitted just beyond the critical angle that therefore undergoes the maximum number of reflections to reach the detector.

The average path of a photon received by the detector and emitted at a distance d is represented by the same distance d divided by the sine of the average angle of emission, since the angular distribution is uniform the probability of emission between two angles, calculated from the normal to the LSC surface, follows a cosine rule

$$P_{\Delta_\theta} = \cos(\theta_{avg}) = \frac{\cos(\theta_{min}) - \cos(\theta_{max})}{2}$$

substituting the critical angle as θ_{min} and $\pi/2$ as θ_{max} (because the straight path is parallel to the surface), θ_{avg} becomes

$$\theta_{avg} = arcos(P_{\Delta_{\theta_{ca}}}) = arcos\left[\frac{\cos(\theta_{ca})}{2}\right] \quad \text{with} \quad \cos(\theta_{ca}) = \sqrt{1-\frac{1}{n^2}}$$

if PMMA is considered as the transparent medium then $\theta_{avg} \approx 42.2°$ so the contribution of the LSC thickness to the optical path length becomes

$$D = \frac{1}{\sin(\theta_{avg})} = \frac{1}{\sin\left[arcos(P_{\Delta_{\theta_{ca}}})\right]} = \frac{1}{\sqrt{1-P_{\Delta_{\theta_{ca}}}^2}} = \frac{2}{\sqrt{3+\frac{1}{n^2}}} \Rightarrow D_{PMMA} \approx 1.077$$

Albeit being a correction factor to account for the LSC thickness, *D* depends only on the refractive index while the physical thickness of the LSC is related to the number of reflections but not to the length of the path.

Putting all the corrections together, the expected intensity at a given distance taking when another measure is taken as a reference becomes

$$I = I_0 M D \frac{\gamma}{\gamma_0} = M D \frac{\arctan\left(\frac{l}{2d}\right)}{\arctan\left(\frac{l}{2d_0}\right)}$$

where I_0 is the intensity measured at the reference distance d_0 and l is the width of the detector (400µm for the optic fibre used in this work).

5.1.4 Output spectra comparison

In order to have an outlook about the behaviour of the LSCs employing different dyes, the first measures were taken using a constant acquisition time of 45ms while the lighted spot have been positioned at distances of 50mm, 100mm, 150mm, 200mm, 240mm from the border.

With these parameters the measures taken from all the samples can be fairly compared without the need for corrections related to the saturation of the photodiodes as well as the different noise levels.

All the LSC samples used for this test are made of PMMA doped with 300ppm of dye, the dye is added to MMA before polymerization, the result are LSC slabs with a size of 3×2m and a thickness of 5mm (4mm for the yellow dye) that are later cut by mean of a laser cutting machine that cuts PMMA with a good quality of the edges.

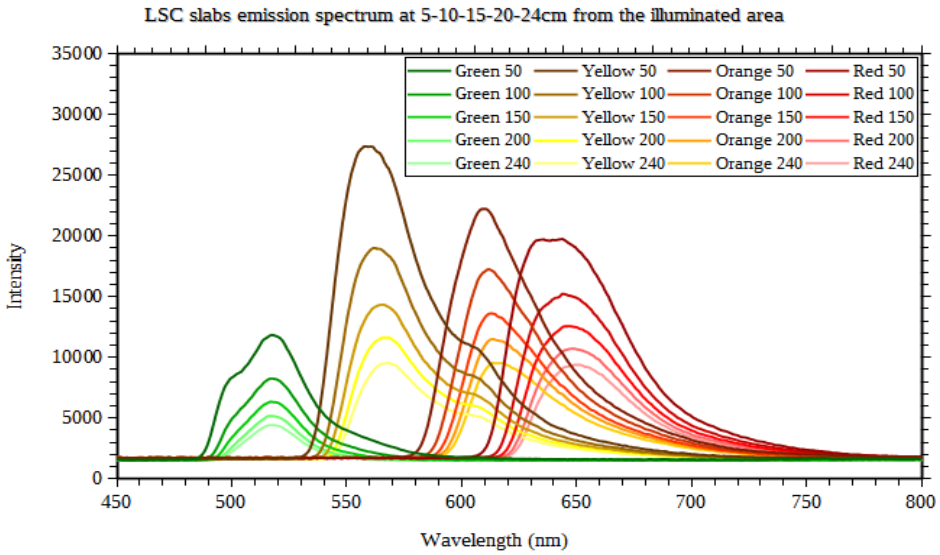

All the measures are relative to samples cut from the same batch in order to minimize the

differences in the manufacturing process of the slabs which doesn't represent the subject of this work.

As we can see the green dye performs poorly because the emission is significantly lower compared to the other dyes, even if the smaller absorbable portion of the solar spectrum is taken into account.

The emission intensity of the yellow dye is particularly high because of the smaller thickness of the slab which results in a 20% higher concentration factor. The red and orange dyes emit with a similar intensity with the orange dye having a sharper emission curve.

In the following graphs are shown the emission spectra of each LSC slab at increasing distances from the side, this measures can provide an evidence of how the self-absorption process affects the LSC output spectrum depending on its size.

In addition, for each dye is provided a comparison between the overall signal intensity measured by the spectrometer and the expected intensity calculated as previously described in Chapter 5.1.3.

5.1.5 Lumogen Green 850

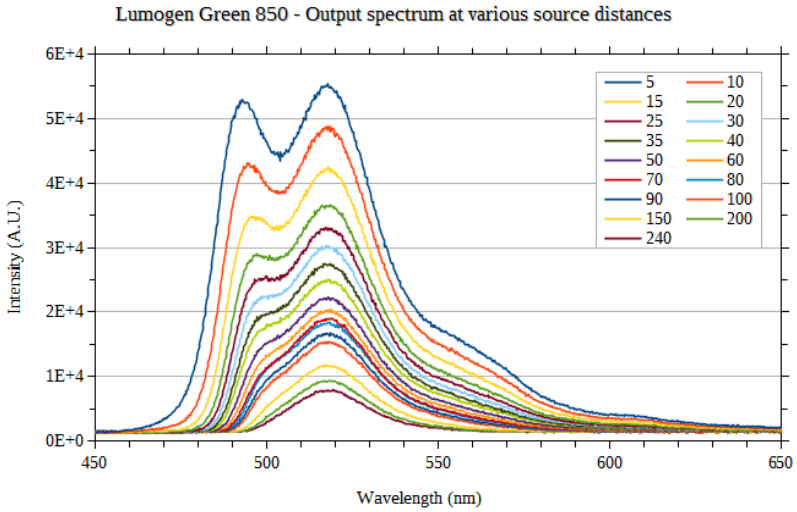

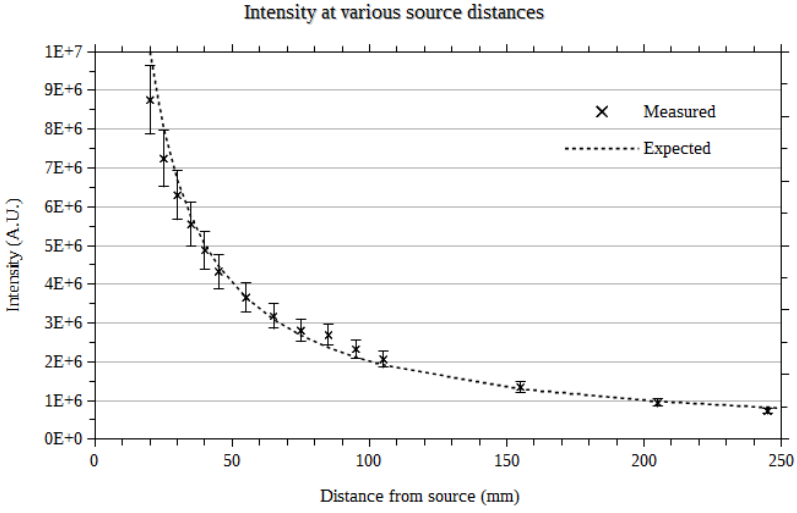

Lumogen Green 850 shows two emission peaks, the strongest one at 517nm and a smaller one at at 494 but the peak at 494nm disappears at longer distances due to self-absorption at the shorter wavelengths.

Self-absorption is strong at wavelengths below 500nm while at longer wavelengths is absent or with a negligible effect because the main emission peak at 517nm maintains its spectral distribution at all distances.

Starting from 150mm, the shape of the emission curve stops changing due to self-absorption therefore this point can be taken as the distance at which all the absorbable

photons are removed from the emission spectrum.

This result means that in systems with an average path length of the photons much longer than 140mm the self-absorption effect can be, in a first approximation, ignored and the system can be modelled substituting the emission spectrum of the dye with the emission spectrum of the LSC at 140mm.

This is obviously a rough approximation because the first centimetres of LSC closer to the cells will provide more light than the rest of the system, but is anyway a good starting point especially in LSCs with reflective surfaces where the average path length of the photons is particularly long.

Despite the strong self-absorption the expected intensity curve fits well the experimental points, this is an unexpected behaviour because the two curves should start to diverge at distances shorter than 140mm.

5.1.6 Lumogen Yellow 083

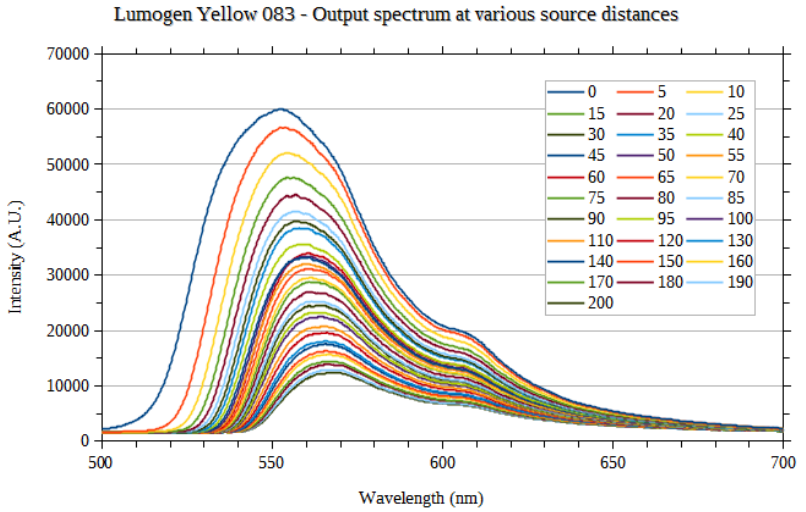

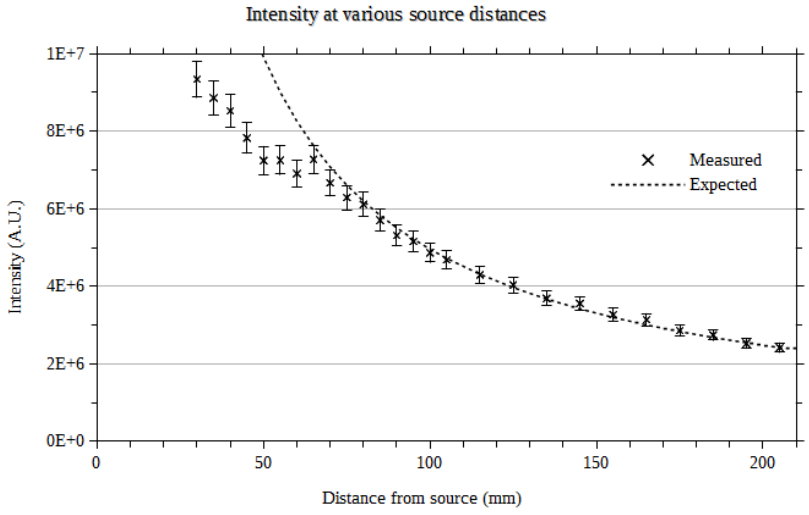

The emission of Lumogen Yellow 083 doesn't show the strong self absorption seen before in Lumogen Green 850 and the comparison between the measured intensity values and the expected ones shows a good agreement starting from 65mm.

This is a much better value than the 140mm distance for the green dye so the yellow dye should perform much better in large area LSCs especially if reflective sides are used.

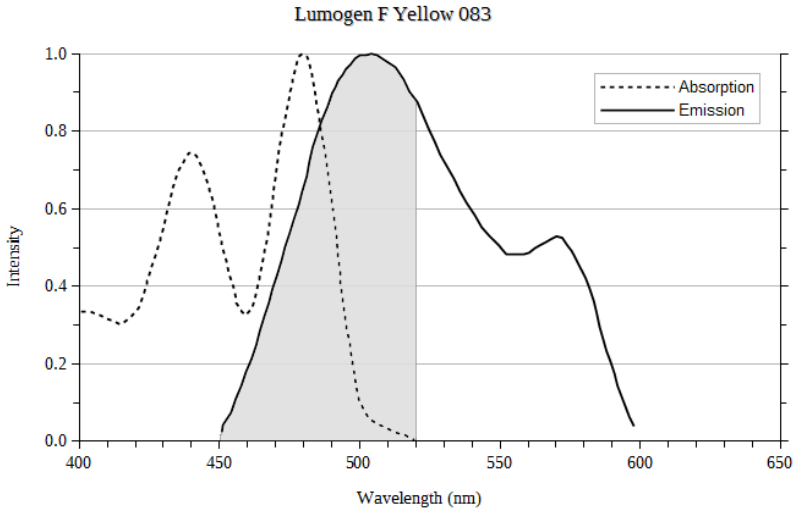

Fig. 5.1.2: Lumogen F Yellow 083 absorption and emission spectra, the area painted in grey represents the output spectrum that could be re-absorbed. Source [13]

The absorption and emission spectra show a partial overlap, the part of the emission spectrum not overlapping the absorption spectrum corresponds to the output spectrum of the LSC when the light source is far from the side.

5.1.7 Lumogen Orange 240

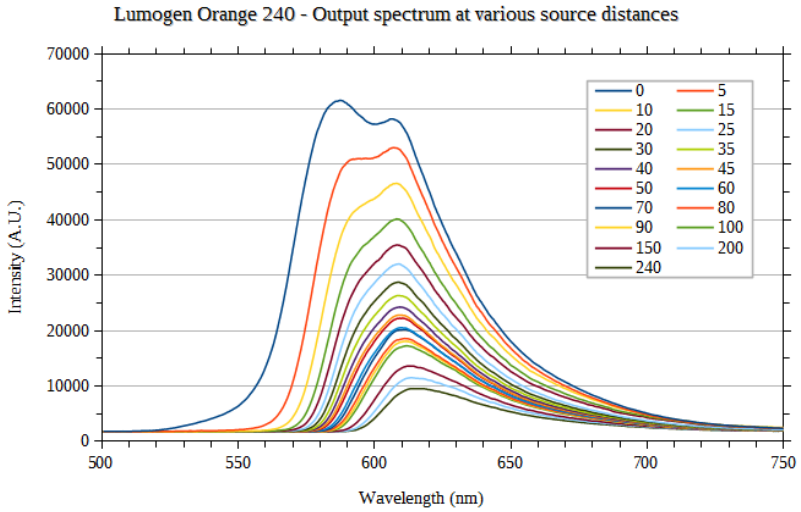

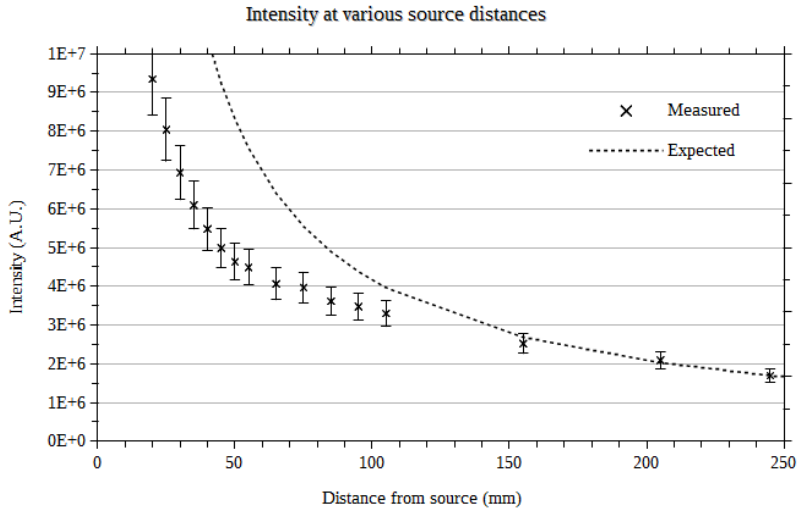

The Lumogen Orange 240 dye shows a strong emission but an equally strong self-absorption, at the shortest distance the emission peak corresponds to 587nm but this band of the emission spectrum is immediately absorbed and at the following distance the peak has shifted significantly by 20nm to longer wavelengths.

At the maximum distance from the side the emission peak corresponds to a wavelength of 614nm.

At all the distances the output spectrum changes in shape and there is almost no agreement between the measured intensity values and the expected ones, this behaviour

suggests that self-absorption is occurring at all distances so the aforementioned approximation can't be considered valid for LSC employing this dye.

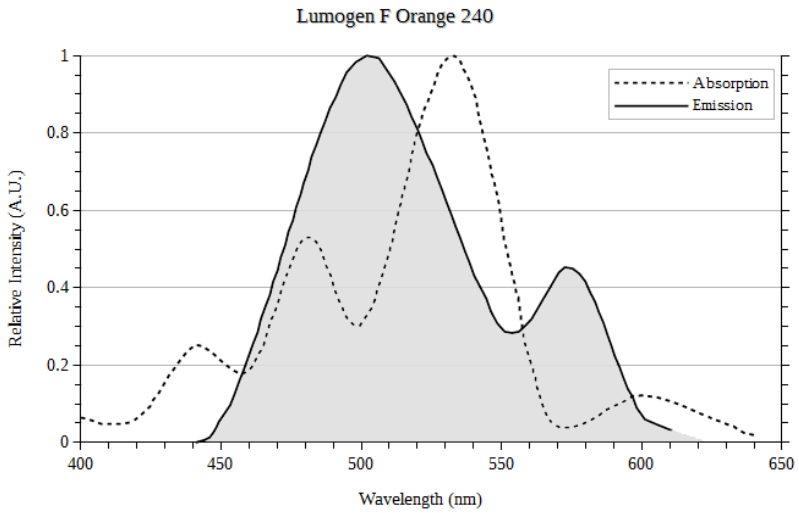

Fig. 5.1.3: Lumogen F Orange 240 absorption and emission spectra, the area painted in grey represents the output spectrum that could be re-absorbed. Source [14]

Looking at the comparison between the absorption and emission spectra we can see a complete overlap of the two curves: this means that all the emitted photons can be re-absorbed leading to the behaviour described in the previous page.

5.1.8 Lumogen Red 305

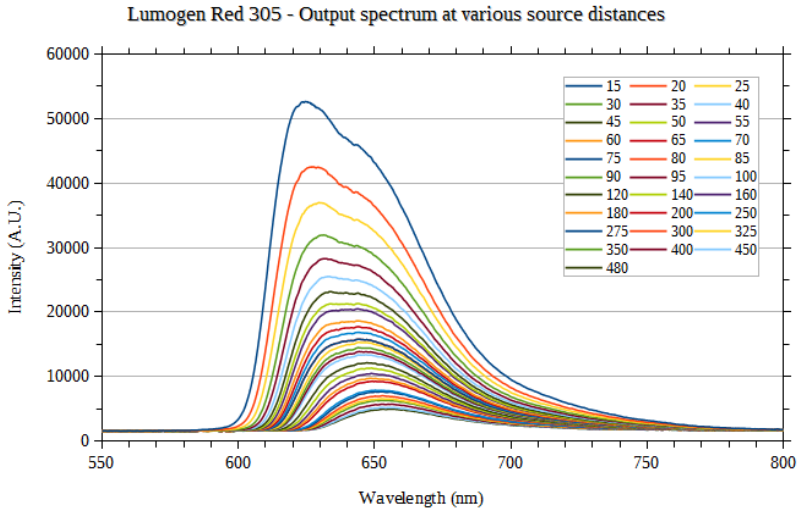

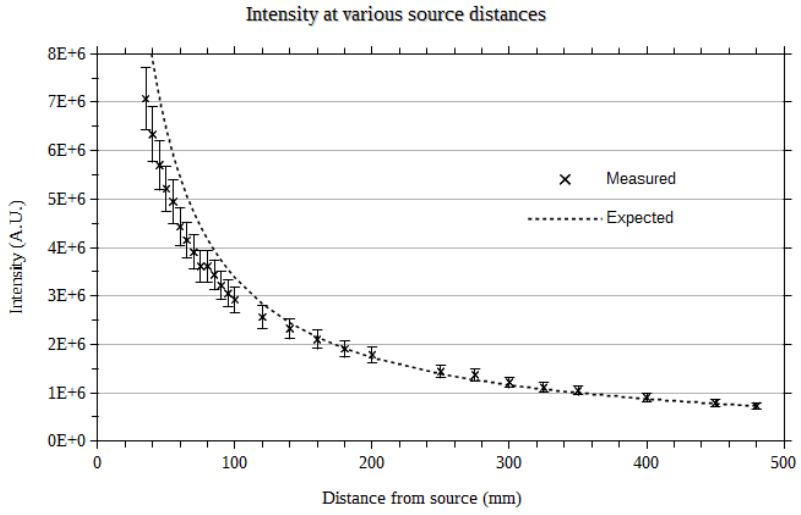

Lumogen Red 305 is the dye most commonly employed in LSC fabrication, it shows a moderate amount of self absorption up to 120mm, beyond this distance the measures of intensity present a good agreement with the expected values.

This sample have been measured at distances up to 490mm therefore the good agreement with the expected values in the 120-490mm range strongly supports the validity of the large LSC approximation.

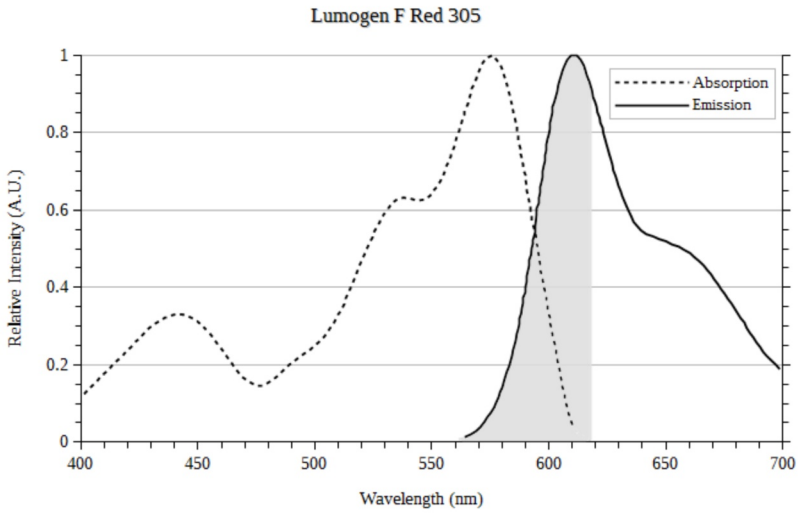

Fig. 5.1.4: Lumogen F Red 305 absorption and emission spectra, the area painted in grey represents the output spectrum that could be re-absorbed. Source [15]

5.1.9 Conclusions

The measures of the output spectrum show that the path length of absorbable photons inside the LSC for three of the four dyes tested is reduced to a few centimetres: 14cm for the green dye, 6.5cm for the yellow dye and 12cm for the red dye. The orange dye have shown evidence of self-absorption at all the distances considered.

This behaviour permits to model LSC larger than the maximum path length of absorbable photons using the emission spectrum of an LSC at that length instead of the full emission spectrum of the dye.

Among the dyes that have been evaluated, green performed poorly with an emission 2.5 times lower than the other dyes, moreover it also presents a strong self absorption making it unsuitable for LSC fabrication.

Hence the most interesting dyes for LSC fabrication are Lumogen Red 305 and Yellow 083 which show a strong emission and a limited self-absorption, Orange 240 could be used but is unlikely to perform well in large systems or in configurations with mirrors.

5.2 Dyes comparison

Among fluorescent dyes the organic ones are the cheaper and most widely available because of their wide use in the manufacturing of plastics goods.

In order to find the best performing, five commercial organic dyes were tested:

- Lumogen® F Violet 570
- Lumogen® F Green 850
- Lumogen® F Yellow 083
- Lumogen® F Orange 240
- Lumogen® F Red 305

The latter four dyes are perylene-based while Violet 570 is a naphtalimide, all of them are widely available on the market and because of their marketed use can be easily mixed with various plastics.

These dyes were added to the MMA used to manufacture the slabs which were subsequently cut into squares of 25×25cm and 50×50cm.

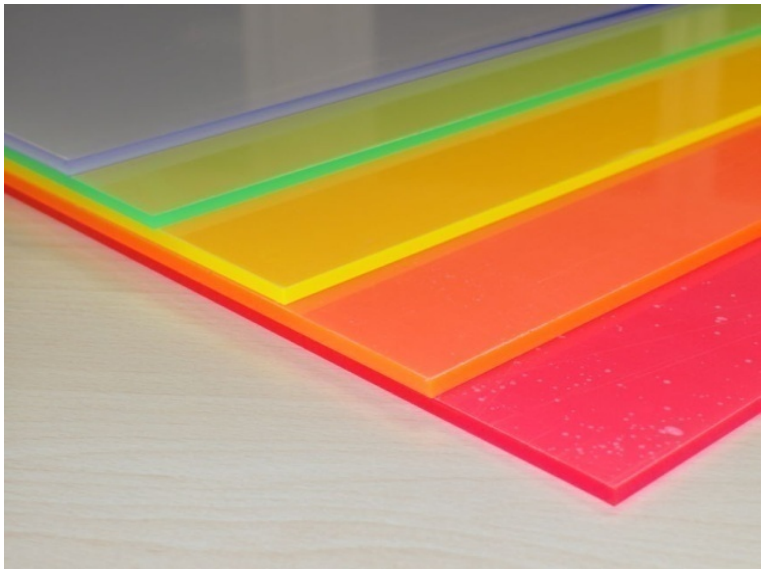

Fig. 5.2.1: The subjects of the study are five types of LSC slabs activated with UV, green, yellow, orange and red dye. These slabs are still covered by a protective film.

Since a few informations are available about large area LSCs it is needed a thorough investigation of the optical properties of the slabs (especially in order to study the self absorption effect) and a careful study of the photovoltaic system to prevent a huge reduction in system efficiency due to a non optimal optical coupling between the slab and

the cells or an increased mismatch in the current produced by the single cells that would severely limit the system efficiency.

The main purpose of this part of the work is the identification of the dye that permits the construction of the most efficient luminescent solar concentrator therefore the samples were manufactured aiming to minimise all the assembly variables in order to get measures dependant mainly on the dye type.

5.2.1 Experimental setup

These LSCs have been coupled with mono-crystalline back-contact back-junction silicon solar cells cut to a size of 23mm by 8mm and soldered onto a printed circuit board (PCB see Fig. 5.2.2) in order to minimize the number of handmade electrical connections and simplify the process of alignment between the slab and the cells.

Fig. 5.2.2: In order to minimize the alignment errors, the cells are soldered onto a printed circuit board in series of 10. For each one of the cells are present test points so them can be tested individually.

Each PCB is 244mm long and hosts 10 cells connected in series, the PCBs are mounted to the LSC sides by mean of an optical glue with a refractive index close to PMMA as described in Chapter 4.2.

Optical coupling between cells and slabs is critical since any gap between the cells and the LSC results in a huge loss of system power. This loss of power is partially caused by the unpredictable reflection of light inside the bubbles in the glue and partially caused by the subsequent increase in current mismatch between the cells.

The area of the cells not covered by the LSC is obscured with black silicone in order to remove this contribution from the measurements (see Fig. 5.2.3). The last 5mm around the perimeter of each slab are covered with a reflective film to protect the surface from glue and silicone.

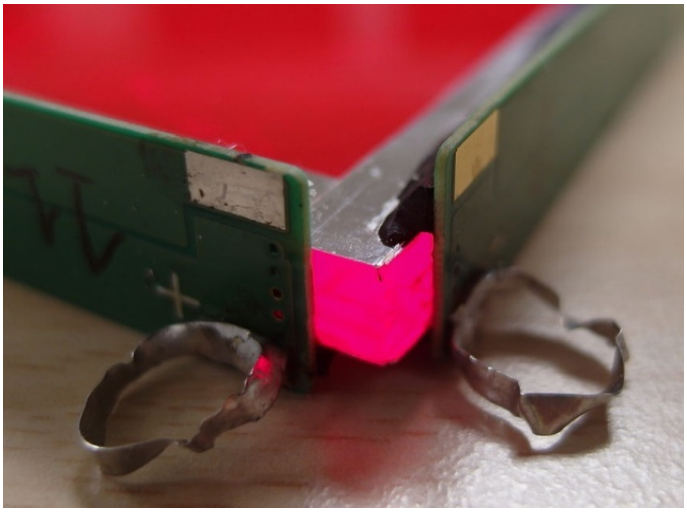

Fig. 5.2.3: Detail of the LSC sides showing the cells PCB, the reflective film and the black silicone. The glowing is the proof that the slab is concentrating the incoming light.

Each 50cm LSC is fitted with 8 receivers (2 per side) and all four sides are connected in parallel: the overall setup is a system of 4 parallel lines of 20 cells connected in series (see Fig.5.2.4).

The prototypes were placed on a sun tracking system equipped with a pyranometer used to measure the global irradiance incident on a plane normal to the direction of sun rays represented by the tracking system itself.

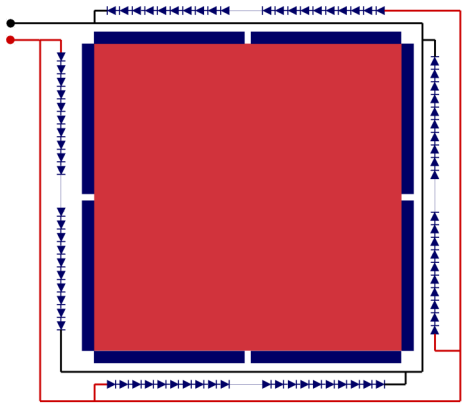

Fig. 5.2.4: Electrical scheme of the cells arrangement in the LSC samples used for the dye evaluation

The IV curves were measured by mean of a Keithley 2400 SourceMeter connected to a computer and controlled by a software written on purpose in LabView (see Fig.5.2.5) which automatically calculates all the parameters of the curve like short circuit current, open circuit voltage, maximum power point, voltage and current at maximum power point

and fill-factor. The software saves automatically the IV curve data and can perform 4-wire measures as well as batch and periodic measures.

The efficiency of the prototypes were obtained later analysing both the IV curves and the irradiance data measured by the pyranometer.

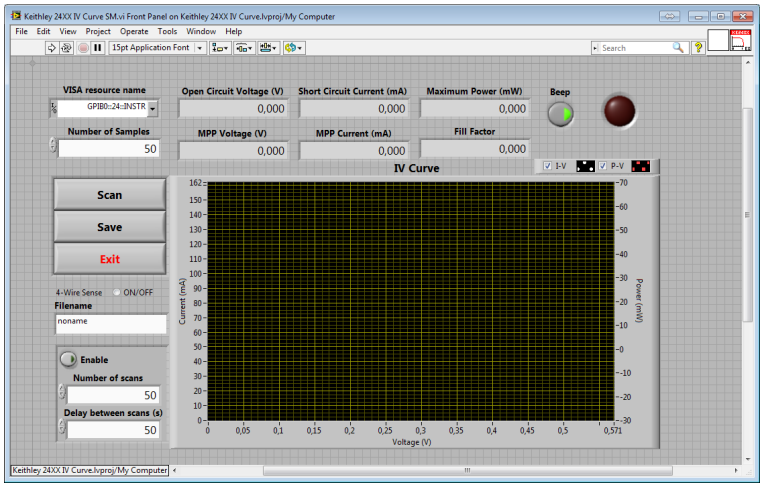

Fig. 5.2.5: The measures have been carried out with a Keithley 2400 SourceMeter commanded by a software written in LabView

5.2.2 Electrical performance

The assessment of the electrical performances of the panels is made by measuring the IV curves of the systems: five 50×50cm LSCs as well as two 25×25cm (red and orange) were tested under natural sunlight while placed on a sun tracking system in order to maximize the irradiance.

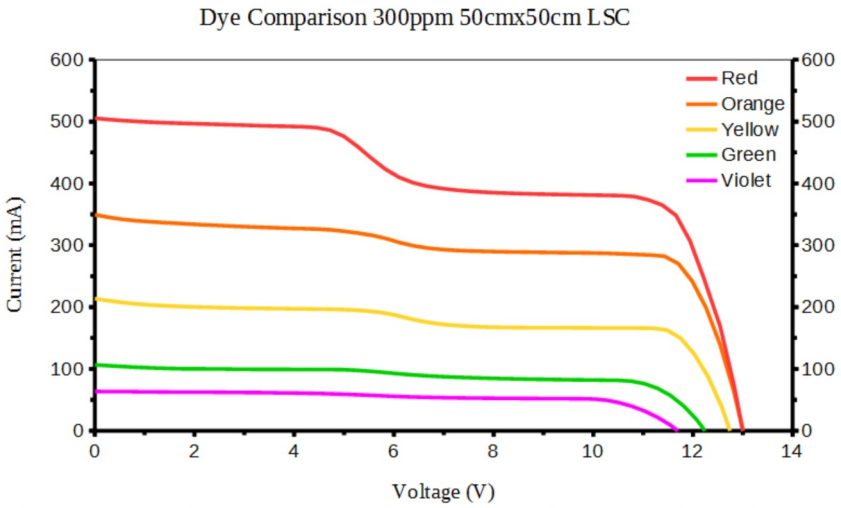

Fig. 5.2.6: The IV curves of various tested LSCs: the red dye is clearly the best performing. The humps in the curves are due to the uneven lighting of the cells in this type of setup but is not significant for our purpose.

The IV curves of the systems show a hump (see Fig. 5.2.6) due to the current mismatch between the cells in the centre and the ones on the sides which receive a 30% lower irradiance due to the geometry of the system however this is not an issue for this study since our goal is to compare different dyes and slab sizes.

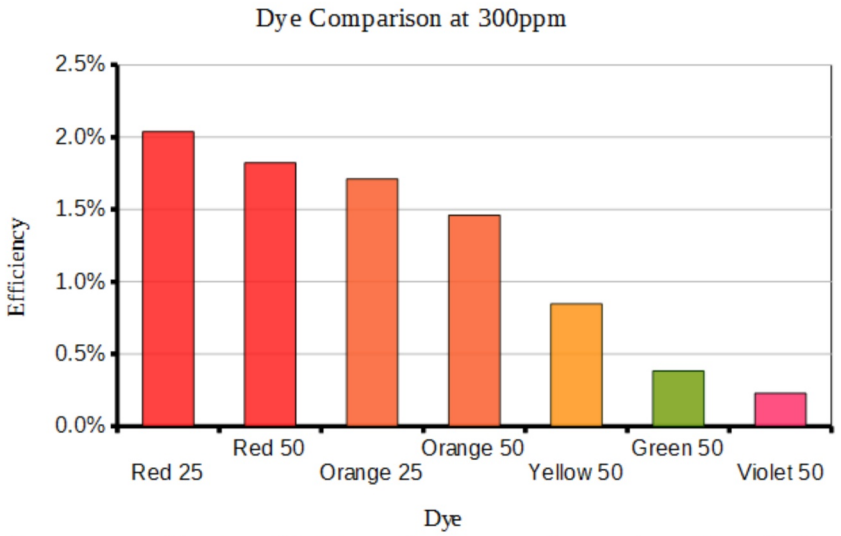

Fig. 5.2.7: A summary of the tested LSCs performances: the numbers 25 and 50 refer respectively to square LSCs with sides of 25cm and 50cm. The efficiency advantage shown by the smaller concentrators is small and mainly caused by the inherent complexity of assembling the bigger systems.

This study confirms that the red dyed LSC is the most efficient due to the higher solar irradiance in its absorption spectrum. Presently green and violet dyed LSCs do not offer significant performances and are worthy only for aesthetic purposes.

5.3 Configurations with reflective sides

Analysing the simulations described in Chapter 3 the designs whose performance appears to be worth constructing a prototype are those with one side equipped with solar cells plus three sides reflective and with two opposed sides with solar cells and the other two sides reflective. While prototypes with solar cells on all four sides have been also been assembled as a reference.

The prototypes were assembled in the same way as described in Chapter 5.2.1 but in this case only LSCs doped with 300ppm of Lumogen Red 305 dye were tested and the receivers were connected in series.

5.3.1 25cm square – solar cells on four sides

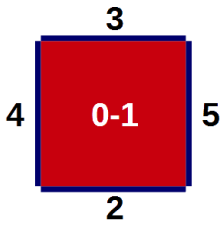

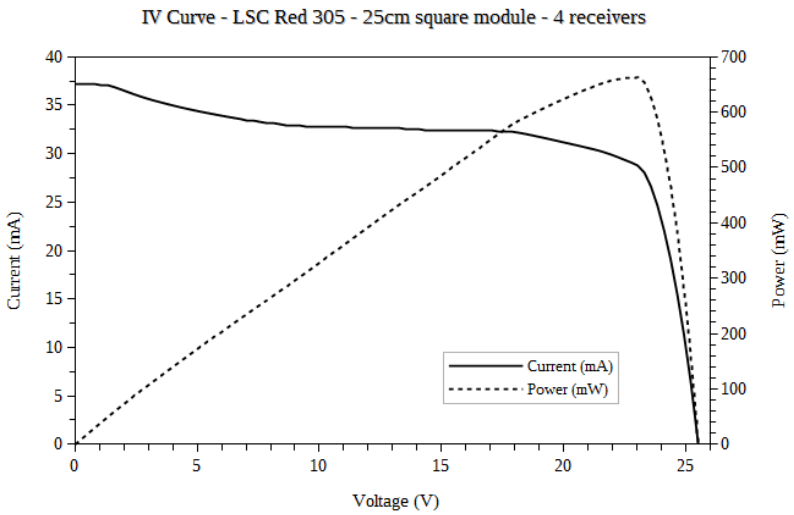

V_{OC} (V)	I_{SC} (mA)	P_{MAX} (mW)	V_{MAX} (V)	I_{MAX} (mA)	Fill Factor	GNI (W/m^2)	Efficiency
25.55	37.16	663	23.03	28.79	0.698	630	1.83%
25.91	49.30	938	23.36	40.18	0.735	830	1.96%

The prototype with receivers on all four sides is taken as a reference, as foreseeable looking at the simulations, in the IV curve is present a hump caused by the mismatch in the current produced by the extreme cells and the ones at the centre of the sides.

Taking as a reference the short circuit current and bearing in mind that the exposed surface of the cells is only 5mm out of 8mm is possible to obtain an estimate of the irradiance received by the cells at the far ends of the receivers.

The estimate for the irradiance at the corners is $I \approx 1.2 \cdot I_0$ with I_0 representing the irradiance on the LSC surface while for the central cells this value increases to 1.67 as in the irradiance profile described by 3.1.1.

5.3.2 25cm square – solar cells on two sides

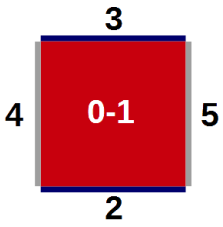

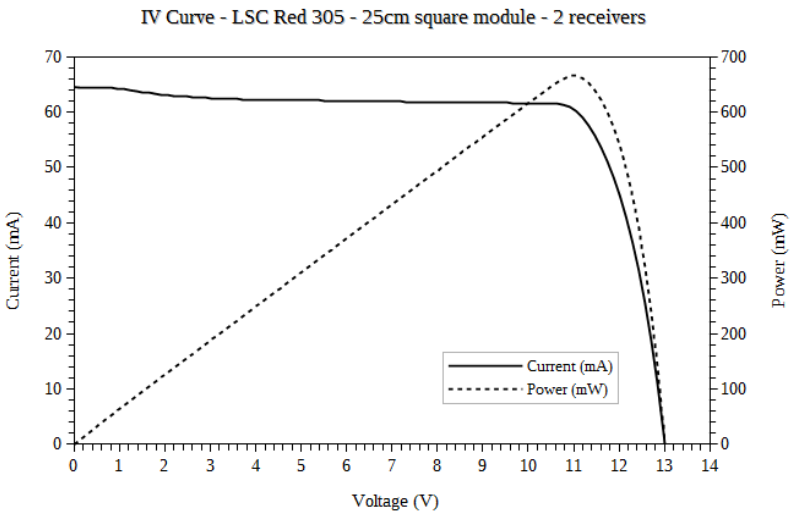

V_{OC} (V)	I_{SC} (mA)	P_{MAX} (mW)	V_{MAX} (V)	I_{MAX} (mA)	Fill Factor	GNI (W/m^2)	Efficiency
13.06	64.54	665	11.05	60.22	0.792	600	1.93%
13.35	97.35	1044	11.33	92.17	0.803	830	2.18%

Looking at the configuration with two receivers the IV curve is much more regular than the reference but the remarkable result is the (albeit limited) increase in efficiency and power production with respect to the reference configuration using only half the cells and with a much simpler wiring.

A small amount of current mismatch appears to be present anyway, this is probably caused both by a reflectivity of the mirror film lower than expected reducing the irradiance on the cells close to it and by the bending of the receivers that makes difficult to glue correctly the solar cells at the far ends of the receiver.

In this configuration the short circuit current scales almost linearly with respect to the reference configuration, in particular the increase in concentration is 1.97X while the irradiance is $2.36 \cdot I_0$.

5.3.3 25cm square – solar cells on one side

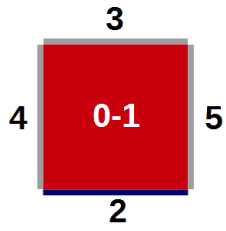

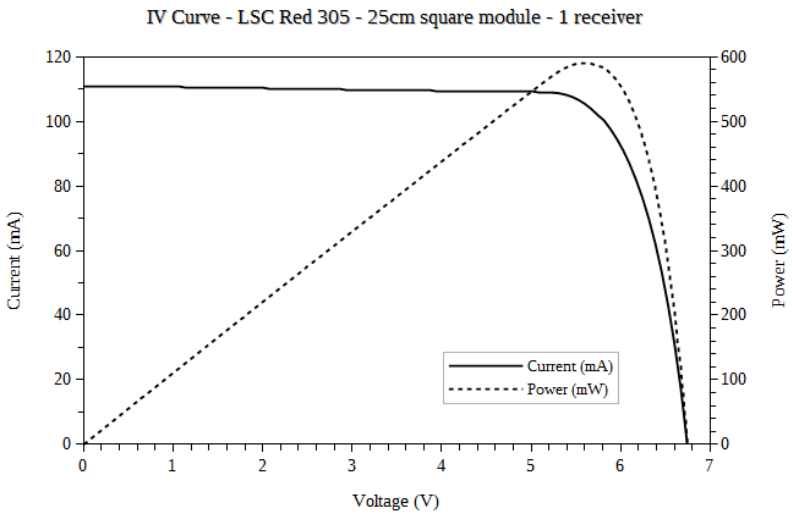

V_{OC} (V)	I_{SC} (mA)	P_{MAX} (mW)	V_{MAX} (V)	I_{MAX} (mA)	Fill Factor	GNI (W/m^2)	Efficiency
6.77	110.91	590	5.60	105.50	0.787	610	1.68%
6.90	172.78	935	5.71	163.74	0.784	780	2.08%

Even if the efficiency is not as high as in case of the configuration with two receivers this configuration is extremely interesting because the decrease in efficiency is counterbalanced by the easier assembly and the lower cost of the materials, moreover the placement of the cells only on one side greatly simplifies the wiring process, an important aspect in solar panels.

The current mismatch between the cells, if present, is negligible and the fill-factor, thanks to the high irradiance on the cells, is very high for silicon solar cells.

In this configuration, comparing the short circuit current with the other systems, the concentration factor is 3.5X with respect to the configuration with cells on four sides and the irradiance on the cells is approximately $4.2 \cdot I_0$.

On these grounds, the use of solar cells optimized for low concentration applications would have increased the efficiency of this configuration where the back-junction solar cells struggle to drain efficiently the current from the cell [16].

5.3.4 Summary

As the simulations suggested, the mirrors improve greatly the uniformity of the irradiance profile and the system with cells on two sides is the configuration yielding the highest efficiency.

The difference between the simulations and the real performances of the modules can be attributed to a mirror reflectivity lower than expected and to minor assembly errors caused by the bending of the receivers which resulted in a non optimal optical coupling between the LSC and the cells at the far ends of the receivers.

Anyway these tests provided remarkable results because systems assembled using a half or a fourth of the cells used in the reference configuration have demonstrated to provide a similar power output at a fraction of the cost and with improved ease of wiring.

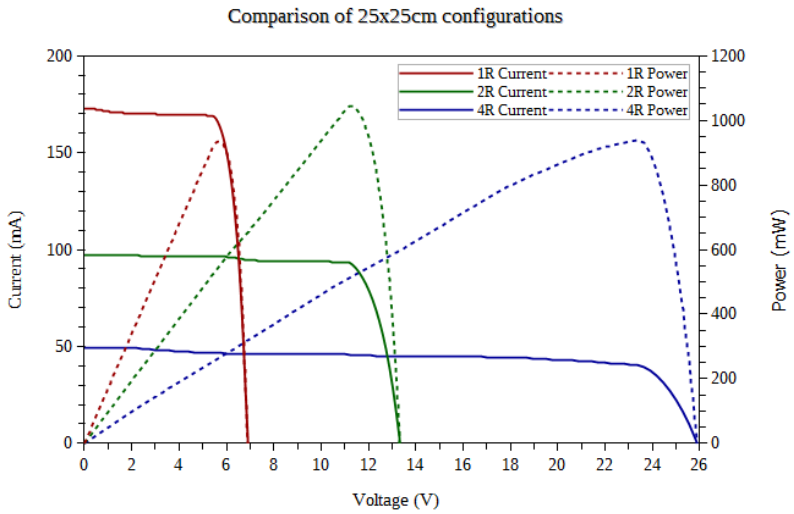

Fig. 5.3.1: The IV and PV curves of the three LSC configurations tested with a GNI of 1000W/m^2 show a good scaling in current production: proof of the increased concentration in modules with reflective sides

The increase in concentration factor shown by the systems employing mirrors is close to the expected values and are 1.97X and 3.5X for the configurations with two and one receiver respectively. These figures could be further improved by a thorough work about the optical coupling of the film to the LSC.

The irradiance on the cells side of the LSC with three reflective borders have been estimated to be 4.2 times greater than the solar irradiance on the LSC surface: this value is non ideal for cells designed to work at one sun, in particular for these tests PERC (Passivated Emitter Rear Contact) solar cells have been used, these solar cells perform well

at 1 sun and up to 2-3 suns but at higher irradiance levels their performance decrease sharply [16] because are not designed to conduct high currents through the cell.

Employing solar cells designed to work at low concentration levels would provide a higher efficiency in configurations with three reflective sides, especially if bigger concentrators are taken into account.

5.4 Impact of shading

Unlike the solar systems aimed at centralized production that are employed in large power plants, the modules for building integration are likely to be subject to shading when not used in roofing applications.

This shading can be caused by trees or other buildings and is also likely to have seasonal variations therefore robust designs with reduced shading losses are preferable for building integration.

Systems using cells connected in series are very sensitive to shading due to the associated current mismatch, it is possible for a setup performing well when uniformly illuminated to drop in efficiency more than other configurations when partially shaded because the shaded cells limit the current produced by the whole systems.

The same systems assembled as described previously were tested under some significant shading situations in order to assess how sensitive to shading are the different designs, in particular the simulations have shown as the configurations with many mirrors should perform well under shading because the multiple reflections inside the LSC help to even out the irradiance profile on the cells.

High power modules can even suffer permanent damage when shaded because the shaded solar cells connected in series with fully exposed ones become reverse biased leading to hot spot damage if bypass diodes or other bypass devices are not installed to protect the cells.

In order to maximise the effect of shading, the tests were performed covering half of the concentrator with black velvet: this precaution is needed to avoid that the light emitted by self absorption and is lost from the escape cone could be reflected back by the shading surface.

Covering half of the system is obviously a situation of extreme shading which a proper installation of the modules should avoid but the modules working fairly in this situation could be used on purpose in a context where partial shading is unavoidable and where the installation of other systems would be economically infeasible.

Depending on the arrangement of the cells in the concentrator it is possible to identify different shading situations:

- In the reference system equipped with four receivers, being symmetrical on two axes, any shading mode is equivalent
- In the system with two receivers on opposing sides two shading options are possible, across the receivers and parallel to the receivers, given the symmetry of the system it is not important which receiver is being shaded.

- In the system with only one receiver three options are possible, the first one involves shading across the receiver, the second one shading along the receiver on the half surface without the receiver and the third one shading the half surface which includes the receiver.

5.4.1 25cm square 4 receivers

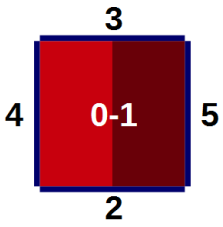

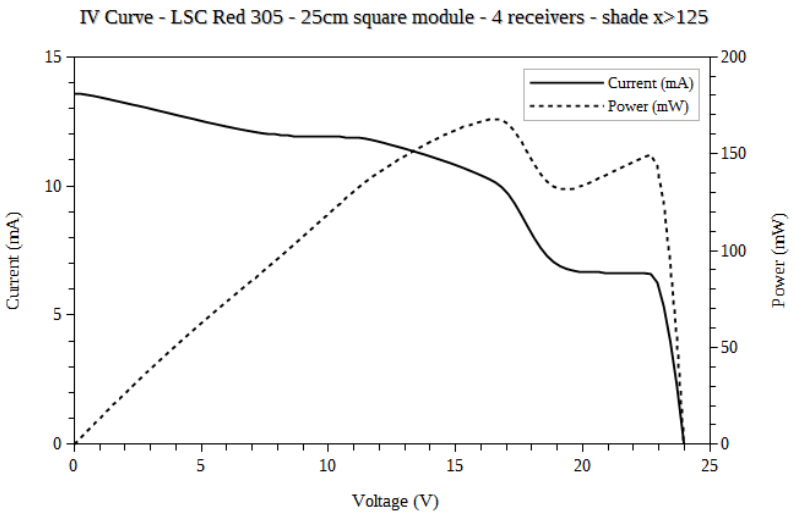

V_{OC} (V)	I_{SC} (mA)	P_{MAX} (mW)	V_{MAX} (V)	I_{MAX} (mA)	Fill Factor	GNI (W/m^2)	Efficiency
24.02	13.54	168	16.56	10.14	0.516	630	0.93%

The shading has a dramatic effect on the reference system, two receivers are half shaded while another one is fully shaded, the consequent current mismatch hinders the performance and the efficiency is halved with respect to full exposure.

5.4.2 25cm square 2 receivers

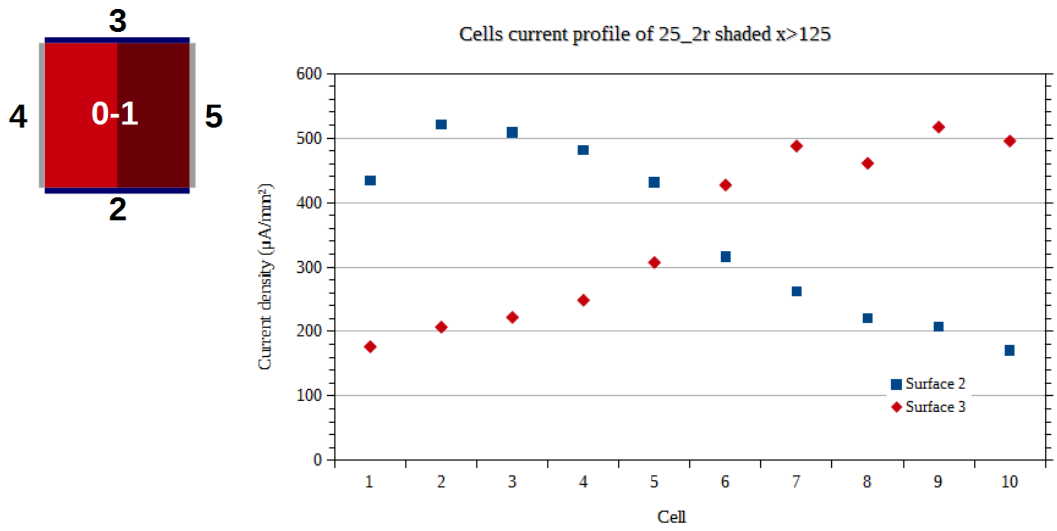

As expected looking at the results of the simulations, the highest current is produced by the cells 2-3-4 while the minimum is produced by cell number 10, the receivers are not symmetrical so the cells of the receiver placed on surface 3 are numbered backwards.

The difference in current production is not as high as expected because of the reflectivity of the sides which is lower than expected value used for the simulations.

Since both the cells and the receivers are connected in series, the cells at the shaded far end of the receivers (n.10 for surface 2 and n.1 for surface 3) are the limiting factor for the system power production.

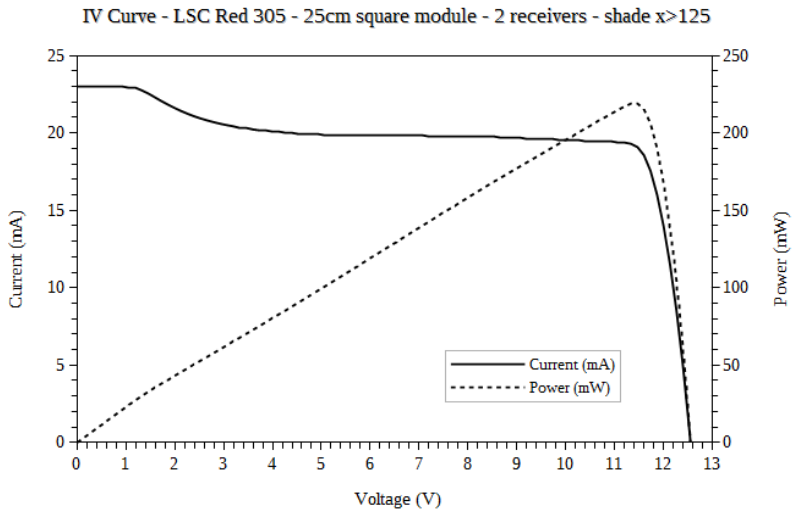

V_{OC} (V)	I_{SC} (mA)	P_{MAX} (mW)	V_{MAX} (V)	I_{MAX} (mA)	Fill Factor	GNI (W/m^2)	Efficiency
12.58	23.01	219	11.47	19.09	0.757	620	1.23%

It appears evident that this configuration performs much better than the reference, despite the non uniform illumination of the cells the fill factor is high and the efficiency is only 50% lower with respect to the unshaded configuration.

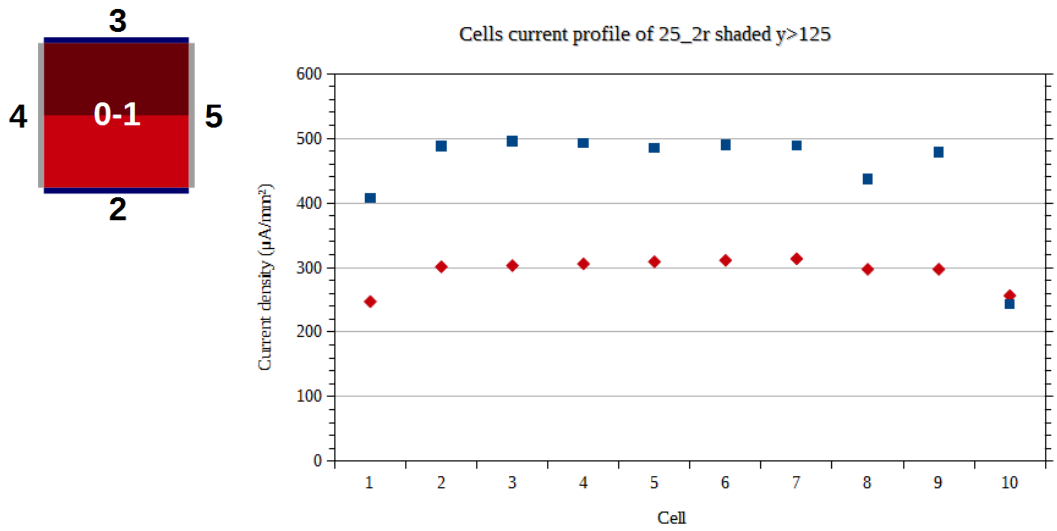

In this case the current profiles of the receivers are much more uniform, a very important aspect is that, even if one receiver is completely shaded and thanks to the uniform irradiance profile, the cells producing less current and therefore limiting the overall system power production are anyway producing more current (25mA vs 19mA, a significant 32% increase) than in the previous case.

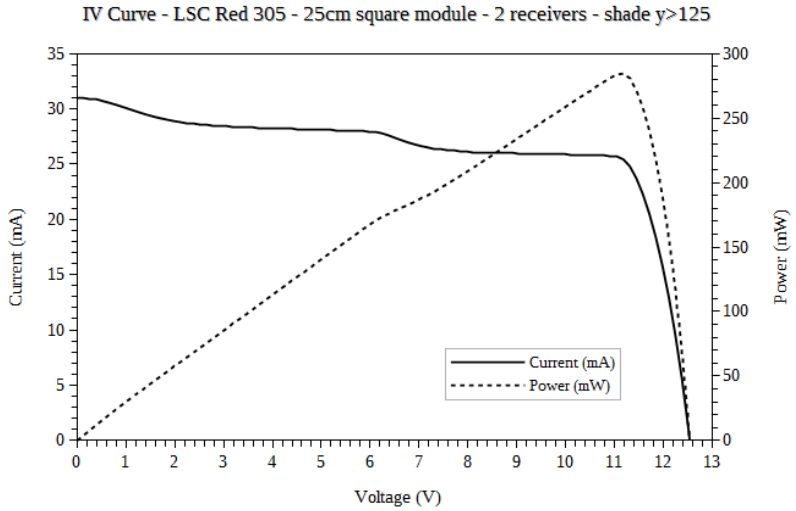

V_{OC} (V)	I_{SC} (mA)	P_{MAX} (mW)	V_{MAX} (V)	I_{MAX} (mA)	Fill Factor	GNI (W/m^2)	Efficiency
12.55	31.02	285	11.18	25.44	0.731	620	1.59%

As expected the efficiency is just 20% lower than in the unshaded condition but the remarkable result is that with half of the receivers this configuration is producing a 69% higher power output than the reference.

5.4.3 25cm square 1 receiver

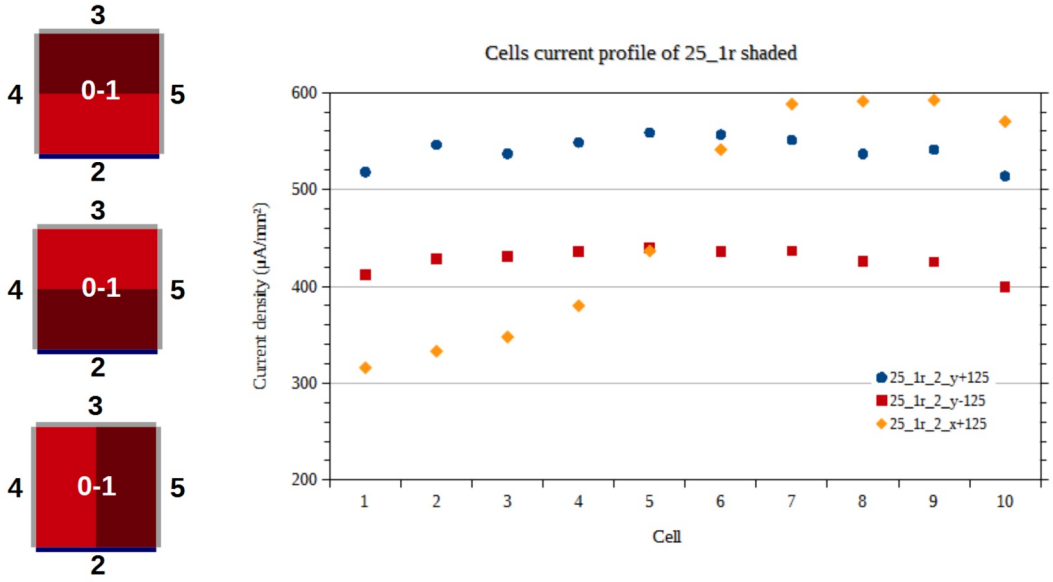

Looking at the results obtained through the simulations, this configuration is clearly the most promising because it is expected to be the most efficient under all the shading conditions considered.

Having only one receiver three shading configurations are possible and as previously observed the most critical one involves the shading of half the receiver.

A remarkable result is the good agreement between the irradiance profile obtained by the simulations and the current profile measured in the prototype, as expected there is a ratio of two between the current produced by the best and worst cells across the receiver.

In the other two cases the current profile is quite uniform, with a current mismatch of 10% comparing the cells at the centre to the ones at the far ends.

This mismatch is higher than expected and most likely caused by a mirror reflectivity lower than expected and non optimal optical coupling of the cells at the far ends due to the bending of the receiver.

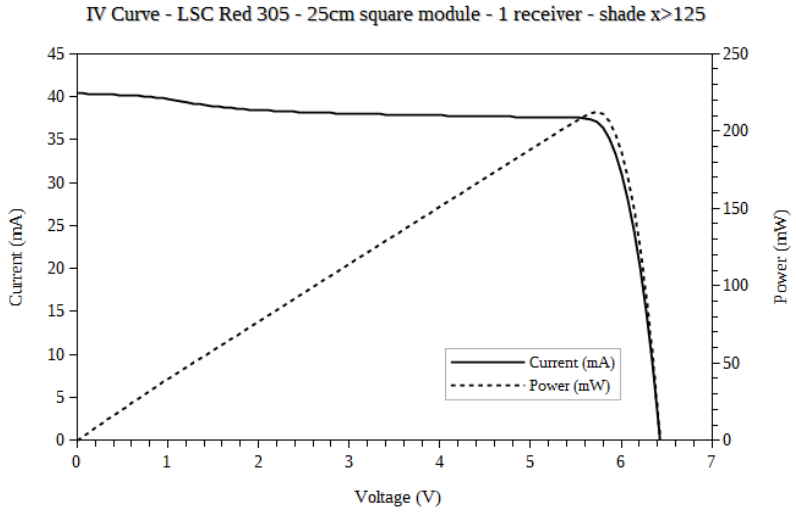

V_{OC} (V)	I_{SC} (mA)	P_{MAX} (mW)	V_{MAX} (V)	I_{MAX} (mA)	Fill Factor	GNI (W/m^2)	Efficiency
6.43	40.40	212	5.73	37.07	0.817	600	1.23%

In the worst case scenario the system is performing remarkably well with a fill factor higher than 80% that is exceptional for silicon solar cells.

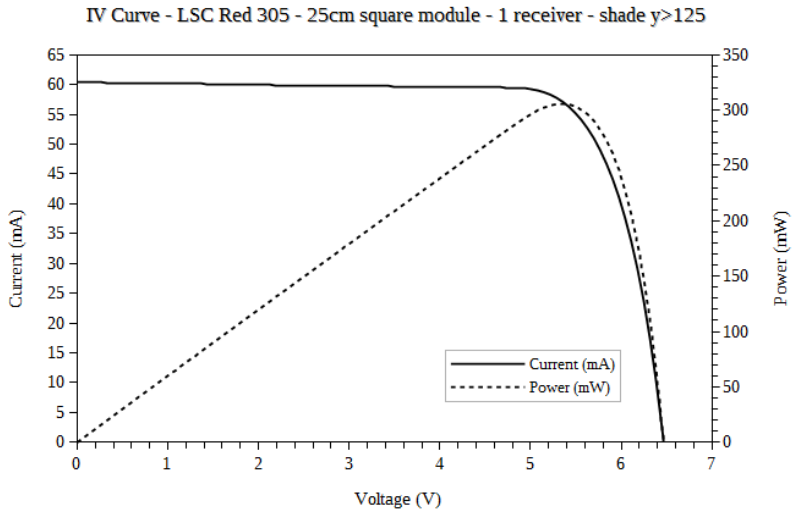

V_{OC} (V)	I_{SC} (mA)	P_{MAX} (mW)	V_{MAX} (V)	I_{MAX} (mA)	Fill Factor	GNI (W/m^2)	Efficiency
6.47	60.37	306	5.35	57.12	0.782	570	1.86%

When the surface opposed to the receiver is shaded, the IV curve of the system is almost impossible to tell apart from that measured in an unshaded condition, in this case the efficiency is even higher because this shading configuration reduces the contribution of self absorption to the overall system efficiency.

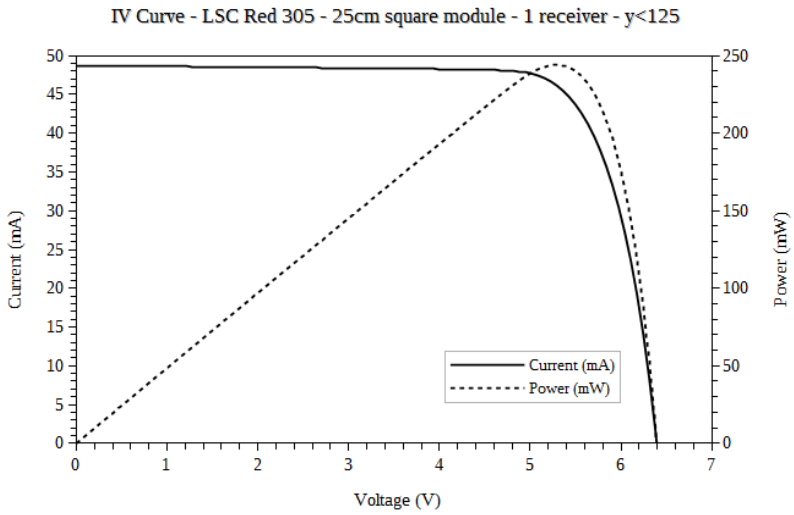

V_{OC} (V)	I_{SC} (mA)	P_{MAX} (mW)	V_{MAX} (V)	I_{MAX} (mA)	Fill Factor	GNI (W/m^2)	Efficiency
6.40	48.72	244	5.29	46.16	0.784	580	1.46%

As in the previous shading configuration is impossible to distinguish this IV curve from the one of the unshaded system, in this case the photons have to travel a longer path before being absorbed.

Since a longer path involves more reflections and a higher chance of self absorption the power production is lower than in the previous case but is anyway a remarkable result for a system whose cells are kept completely shaded.

5.4.4 Summary

These test provided two remarkable results, the first one is the good accordance between the simulations and the measures performed on the prototypes, a difference is present anyway and can be ascribed to the lower than expected reflectivity of the sides and the non optimal optical coupling of the cells at the far ends due to the bending of the receivers.

The second result is that the systems assembled with the reflective film perform very well when shaded, in particular the configuration with the cells on one side have shown the highest efficiency in all shading configurations.

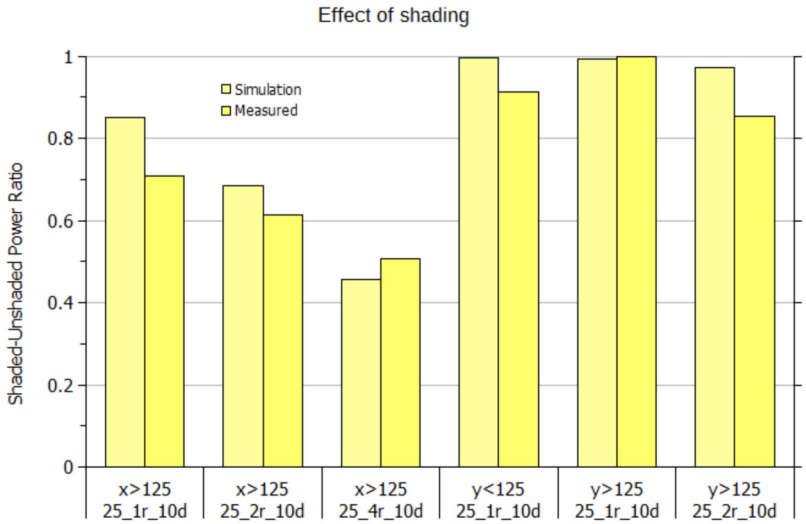

Fig. 5.4.1: Comparison between the efficiency figures obtained through the simulations and the experimental results

LSCs have then be demonstrated as an effective system for building integration in partially shaded locations because their performances are not as heavily affected by partial shading as the traditional modules.

Moreover the designs performing better under partial shading are the ones employing the smallest number of cells, this represents a significant result because any reduction in the number of cells implies not only a lower cost of the components but also a faster, and hence cheaper, assembly process.

6 Applications

6.1 Solar Decathlon 2012 – Astonyshine Project

At Solar Decathlon 2012 that took place in Madrid in September 2012 early prototypes of solar shutters featuring luminescent solar concentrators were installed in the Astonishyne villa [17]: a project proposed by a joint team leaded by the École Nationale Supérieure d'Architecture Paris-Malaquais with the collaboration of the École des Ponts ParisTech, Department of Physics and Earth Science of Università di Ferrara and Department of Architecture of Politecnico di Bari.

Fig. 6.1.1: The solar shutters installed on the Astonyshine house at SDE2012, the photo is taken during the construction of the house

The windows of the house were shaded by couples of shutters 120cm tall by 60cm wide which in the centre hosted a double glazing LSC solar panel of 50×25cm made of PMMA doped with 400ppm of Lumogen Red 305 coupled with monocystalline silicon solar cells placed on all four sides. The energy produced by the system during the daylight hours was stored in a lithium-ion battery and used at night to power an array of white LEDs fitted in the frame of the shutter.

The LSC was integrated in the double glazing panel which had a 5+6+4 configuration composed of the LSC slab itself (5mm thick), an embossed glass with a thickness of 4mm and the spacer between them that was 6mm thick.

6.2 Solar Decathlon 2014 – Liv-lib' Project

The Liv-lib’ project was one of the finalist of the prestigious competition Solar Decathlon Europe 2014 (20 projects have been selected from 17 countries and 3 continents), for the creation of a passive solar house, completely powered by solar energy.

During the final phase of the competition, 20 teams have assembled their own housing prototype at Solar Village in the Palace of Versailles (Paris, France), a great space open to the general public.

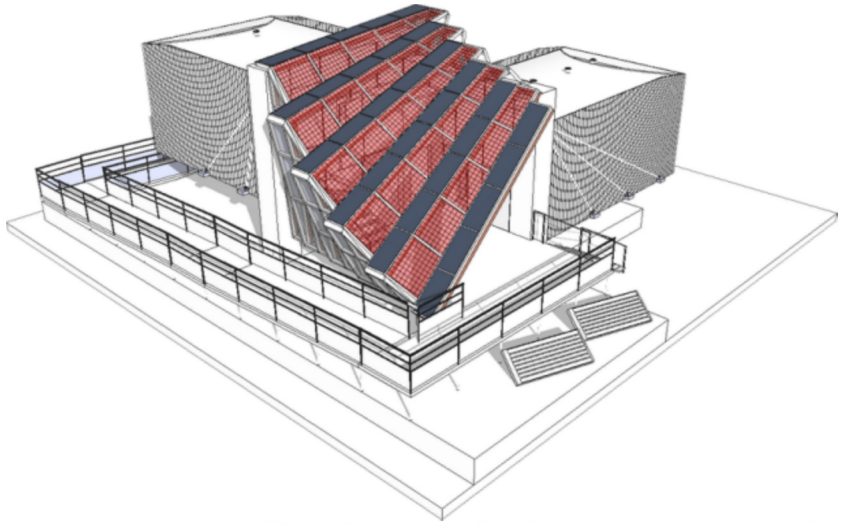

Fig. 6.2.1: Drawing of the Liv-lib' project displaying the LSC panels painted in red and the dark gray thin film CIGS panels

The Liv-lib' project intended to employ a “plug and play» concept into the context of a building. consisting of different distinct elements: the heart of the building, the «hub”, includes all technical services, energy production, distribution and recycling of water, ventilation, etc.

The hubs are connected to “capsules”, removable living spaces or offices, dependent on the «port»: a connection interface. The capsules are designed to be disconnected, transported by truck and connected to another hub, facilitating mobility for inhabitants (see Fig. 6.2.2).

The prototype of Versailles presented a section of one hub and two capsules, a 34 m^2 apartment and a workstation area of 25 m^2. These were connected on the north side of the hub, to leave the south open and well-lit.

Fig. 6.2.2: 3D Rendering of the Liv-lib' project showing a hub with many modules mounted

The south side was also used to satisfy the photovoltaic electricity demand of the house through 30 thin film CIGS (Copper Indium Gallium diSelenide) solar panels with a total area of 21.6 m^2 at 120 Wp/m^2 giving 2.6 kWp and 25 LSC (Luminescent Solar Concentrators) panels with a surface of 23.0 m^2 at 16 Wp/m^2, giving 370Wp for a total power of 2.97 kWp installed (see Fig. 6.2.1).

The Ecole Nationale Supérieure d'Architecture Paris – Malaquais invited the Photovoltaic Laboratory (Department of Physics and Earth Science of Università di Ferrara) to collaborate in their project again, after the successful experience at Solar Decathlon Europe 2012 [17], providing the panels for their novel photovoltaic roof made up of luminescence solar concentrators (LSC).

Fig. 6.2.3: Under the canopy the light gets a red hue caused by the re-emitted light that doesn't undergo total internal reflection

6.2.1 Construction of the prototype

The luminescent slabs used in this project were made of PMMA doped with an organic perylene based dye (Lumogen® RED F 305) that absorbs solar light in the visible spectrum (peak at 577nm) and emits with a peak wavelength of 610nm corresponding to a red colour, a low dye concentration of 300ppm was used to keep the slabs transparent enough to maintain well lit the area underlying the canopy (see Fig. 6.2.3).

Each slab had 3 sides covered with a high reflectivity dichroic film while the fourth side was optically coupled to an array of monocrystalline back-contact silicon solar cells by means of an UV-curing glue, the array of each slab consisted in 5 printed circuit boards (PCB) with 10 cells each (23mm x 7.8mm) connected in series.

The cells were soldered onto PCBs in order to simplify the alignment with the side of the slab easing the assembly process.

In order to fit the saddle shaped surface of the canopy (see Fig. 6.2.4) the 23m^2 covered by the LSC panels were divided in 25 individual modules of 5 different shapes, the modules were connected in series as five strings depending on their shape with the purpose of minimizing the current mismatch.

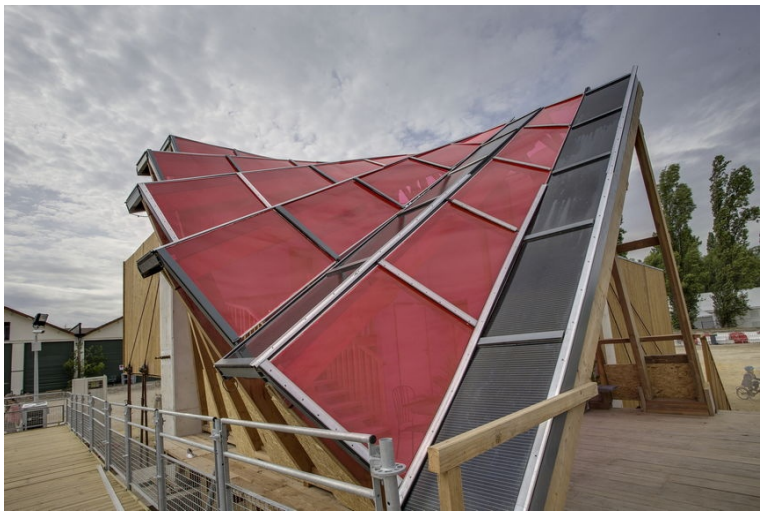

Fig. 6.2.4: Detail of the canopy: the panels were kept in place by aluminium profiles sealed with natural rubber gaskets while the wires ran inside the aluminium extrusions

Each of the LSC strings was connected to an array of Stecagrid 500-MC4 inverters placed in the technical room of the house.

The parts of the canopy facing south were covered by the thin film panels (since they are more efficient) so the LSC were installed in the slope facing east.

6.3 Solar shed at University of Ferrara

This project regards a photovoltaic shed developed at University of Ferrara as a cooperation between the Department of Physics and Earth Sciences and the Department of Architecture. It exhibits many advantages compared to the existing photovoltaic sheds regarding the photovoltaic conversion and a number of additional features.

The goal of this project is the development of a system that is going to be installed at the Scientific-Technological Campus and will allow a sustainable mobility within the campus and towards the other buildings of the University of Ferrara.

The shed is composed by two different structures (Fig. 6.3.1): the first facing south hosts linear LCPV (Low Concentration PhotoVoltaics) modules and shelters the relax area while the second structure faces east (to avoid shading by the campus buildings), is covered with LSC (Luminescent Solar Concentrator) slabs and shelters the charging station for electric bicycles.

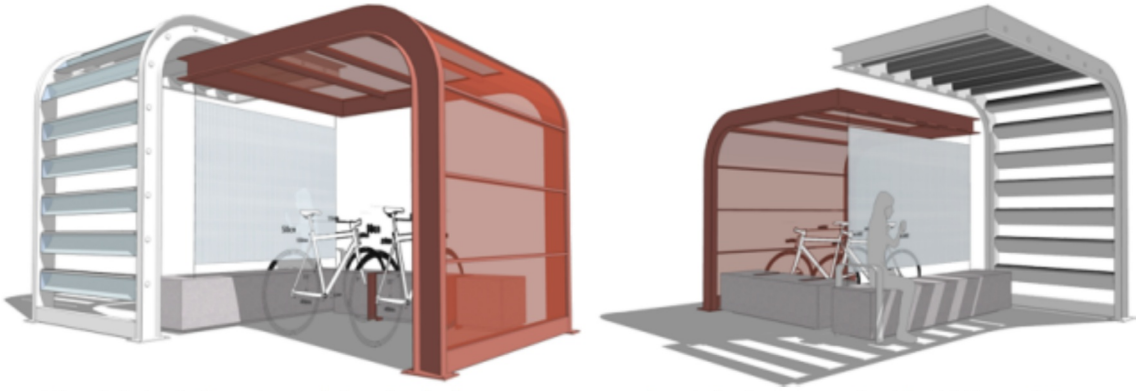

Fig. 6.3.1: A drawing of the shed: the structure on the right is covered with LSC modules and shelters the electric bicycles charging station while the structure on the left hosts the linear CPV modules and covers the WiFi area

The main features of the proposed system are:

- an innovative single-axis low concentration photovoltaic system that couples the energy production function with integrated lighting features.
- static concentrating photovoltaic system based on LSC technology
- charging station for electric bicycles or other small electric vehicles
- WiFi hotspot to connect to the university network
- power plugs to charge mobile devices

6.3.1 Solar F-Light Modules

Solar F-Light LCPV modules have been developed at the Sensor and Semiconductor Laboratory as a joint project with the company GPIII Solar.

These LCPV devices are linear solar concentrators based on a parabolic mirror, the main structure is obtained starting from an aluminium extrusion that presents a parabolic profile, a groove where is placed the protective glass and a slot to host the solar cells. A highly reflective film is placed on the parabolic profile creating the mirror that focuses sunlight on the cells.

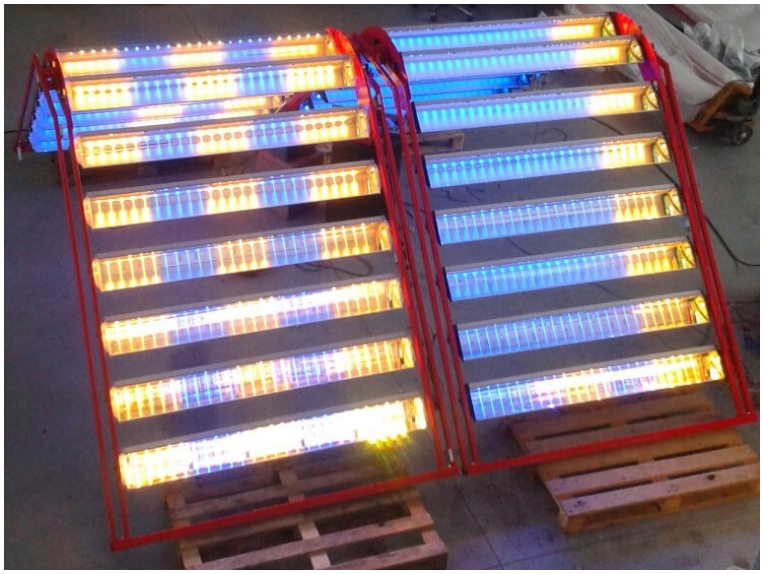

Fig. 6.3.2: The CPV modules are a linear low concentration parabolic concentrator which, in addition to a (daylight) energy production function, may perform nighttime functions as direct and/or diffused lighting, monochromatic and/or colored lighting

The modules are 20cm wide with an optical aperture of 16cm and can be manufactured with an arbitrary length: for the solar shed a length of 150cm (160cm considering the caps) was chosen.

The solar cells used in these devices are back contact monocrystalline silicon cells with a size of 23mm x 8mm and are grouped in arrays of 11 cells soldered on a 30cm long IMS (Insulated Metal Substrate) receiver so each module will have 5 receivers for a total of 55 cells.

Each receiver along with the cells hosts 5 RGB LEDs (RedGreenBlue Light Emitting Diodes) and four connectors (2 for LEDs and 2 for power output) so they can be series-chained in an indefinite number, this is accomplished by using copper wires for power and jumper boards for the LEDs connection,

Each jumper board hosts a led driver with 1-wire communication interface that permits the remote control of the colour and intensity of the light emitted by each receiver (see Fig. 6.3.2).

The aluminium extrusion is closed at the ends by two plastic caps with pivots to allow the rotation of the system, moreover the right cap hosts an electronic board with a microcontroller that performs the sun tracking and relative motor control of the device, controls the LED arrays of the module, integrates tilting sensors and DMX over RS485 communication to permit the complete remote control of the module with an industry-standard interface.

The main feature of this system is indeed the presence of an integrated and advanced lighting system that permits to operate each Solar F-Light in three working modes (Fig. 6.3.3):

- during day-time can follow the sun producing energy and maximizing the shading on the underlying area
- during night-time the RGB LEDs arrays can provide direct lighting using the same parabolic mirror that concentrates light on the cells
- diffused lighting can be obtained by directing the light beam on the underside of the following module.

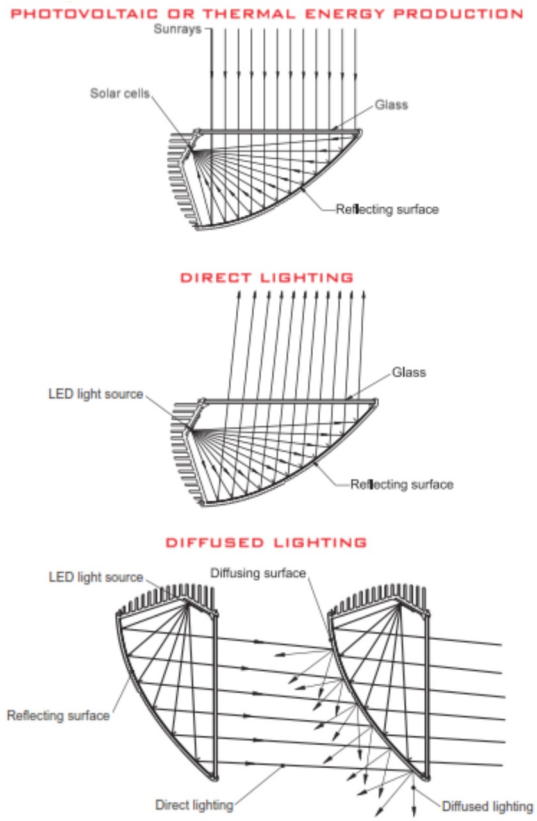

Fig. 6.3.3: The three operating modes of the linear CPV system: energy production (top), direct lighting (middle) and diffused lighting (bottom)

The maximum power output of the LSC subsystem is of 25Wp for each module that multiplied for 13 modules yields 325Wp, being sun tracking modules it must be noted that the power output remains close to this value throughout the day.

These modules will power the electric bicycle chargers: most electric bicycles have batteries with a capacity varying from 150 to 400Wh so two of them can be fully charged in a standard morning with 4h of lessons.

6.3.2 LSC Modules

An LSC solar panel is an innovative device that combines the advantages of concentrating photovoltaic with features well suited to be employed as architectural elements. The Sensor and Semiconductor Laboratory have a good experience with these devices having previously demonstrated the feasibility of large LSC at the international competitions Solar Decathlon Europe 2012 [6.1] and 2014 [6.2] providing two teams with LSC shutters (Astonishyne, 2012) and panels for a canopy (Liv-lib', 2014). (see Fig. 6.3.4)

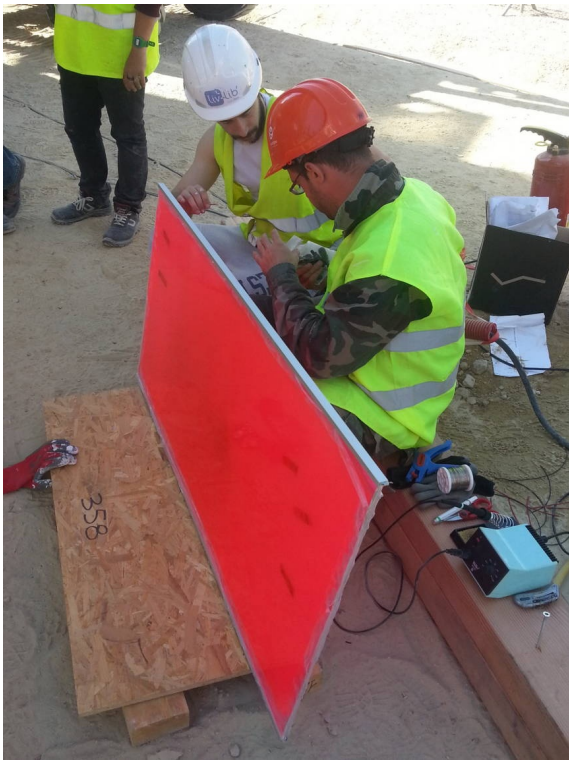

Fig. 6.3.4: A luminescent solar concentrator (LSC) module developed at Physics and Earth Sciences Department of University of Ferrara, the slab is still showing the protective film and the solar cells are enclosed in an aluminum profile

The same cells of the LCPV modules are also used for the LSCs, the only difference is that in this case they are connected in series of 10 and are soldered on a PCB (Printed Circuit Board) instead of an IMS (Insulated Metal Substrate) because the low

concentration of LSC systems do not require the use of an heatsink.

The LSC structure of the shed will be covered by 8 panels 2 meters long and 50cm wide made of PMMA (polymethylmethacrylate) doped with 300ppm of Lumogen® F Red 305 perylene based red dye.

In order to find the best arrangement for the solar cells with this LSC shape a ray tracing simulation have been carried out and as a result the cells will be placed only on one of the long edges covering the other three with a dielectric reflective film. For such a long LSC the installation of the cells on only one side of the device dramatically reduces both the cost and the assembly speed.

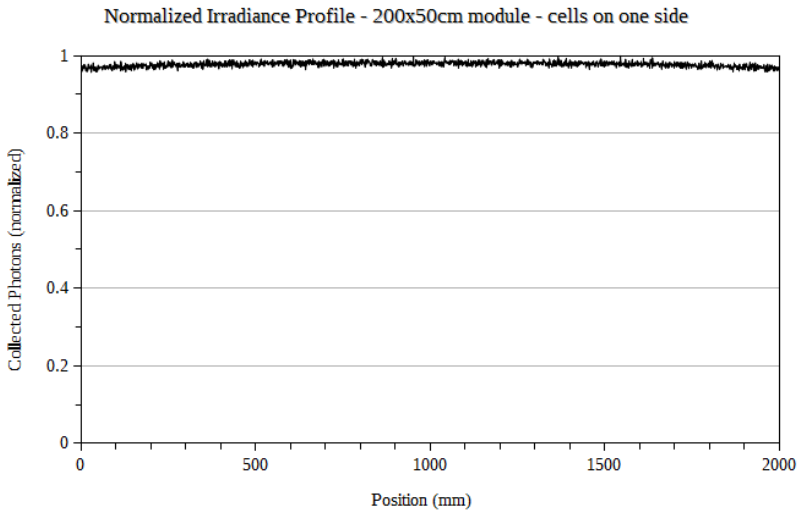

Fig. 6.3.5: Simulation of the irradiance profile on the cells for a 200x50cm LSC with the solar cells placed only on one long side and the other sides covered with a reflective film

Presently these LSC devices have an efficiency of roughly 2% so the peak power output of the installed LSC panels will be 160Wp but given the slope (four arranged horizontally and four vertically) and orientation of the shed (the southern side is used for the LCPV devices) a more realistic estimate is 40W of power output: sufficient to power the wireless access point (6W) and the mobile devices chargers (5W each).

6.3.3 Expected Outcome

This experimental project in the field of production, management and use of energy from sustainable sources pursues the following goals:

- Investigation into the reliability of new technologies which are currently at research stage, in particular long term stability of LSCs has yet to be proven.

- Adoption at the same time and organically of a variety of technologies

- Teaching and educational purposes

7 Conclusions

Luminescent Solar Concentrators are a promising technology well suited for building integration, moreover if installed on the roof of greenhouses they could both reduce power consumption and increase the amount of light available for photosynthesis [18].

Most of the research about LSCs [19] is currently focused on the development of dyes with low self-absorption or dye alignment which purpose is the reduction of the self-absorption losses and the consequent increase in the system efficiency.

Presently the main drawback of LSCs is their low price-per-watt ratio so in order to improve their appealing to the market the efficiency must be increased or price lowered.

The use of solar cells made of semiconductors with a bandgap wider than silicon such as InGaP or GaAs improves the performances effectively but their cost is also much higher than silicon so they can be employed only in LSCs that achieve a high concentration where their high cost is balanced by the high efficiency.

Semiconductors like CdTe and CIGS represent an interesting alternative to silicon but their efficiency when used in LSC devices should be investigated more thoroughly while the availability of monocrystalline silicon solar cells specifically designed for low concentration applications could improve both efficiency and price.

Thin film LSCs layered with glass slabs represent an interesting technology that could allow the use of LSCs in applications where plastic slabs can’t be used, typically where are needed a layered glass or a surface more resistant to scratches than PMMA.

This work is aimed at the optimization of luminescent solar concentrators using technologies and materials already available in order to ease the technology transfer to the industry: the first result obtained is that the feasibility of large size LSCs (up to one square metre) well above the common laboratory size of 5×5cm have been demonstrated.

It has also been shown that the performances of LSC systems can be improved while lowering cost at the same time using reflective layers to get a more uniform irradiance profile on the cells.

Anyway the most remarkable result obtained so far is having demonstrated that systems employing a small number of cells and a reflective film on the remaining sides of the LSC can yield a higher efficiency than a traditional system with cells placed on four sides, moreover these systems have also demonstrated a lower sensitivity to shading losses which represents a fundamental result for a technology targeted at the building integration.

Within this work many prototypes have been assembled and tested, not just in laboratory

but also in an operative environment and international competitions, highlighting the progress of luminescent solar concentrators from a laboratory scale to a promising industrialisable technology.

7.1 Publications

This thesis is based on the data presented in the following works:

Publication

- *Building integrated low concentration solar system for a self-sustainable Mediterranean villa: The Astonyshine house*
  F. Aldegheri, S. Baricordi, P. Bernardoni, M. Brocato, G. Calabrese, V. Guidi, L. Mondardini, L. Pozzetti, M. Tonezzer, D. Vincenzi
  Energy and Buildings 77, pp. 355-363

Oral

- *A Multifunctional Photovoltaic Shed for Sustainable Mobility*
  P. Bernardoni, M. Tonezzer, D. Vincenzi, V. Guidi, S. Baricordi, G. Calabrese
  Proceedings of the 31st European Photovoltaic Solar Energy Conference and Exhibition (EUPVSEC 2015), pp. 2639-2641

- *Building integrated photovoltaic system for a solar infrastructure: Liv-lib' project*
  M. Brocato, R. Zarcone, P. Bernardoni, D. Vincenzi
  SHC 2015, International Conference on Solar Heating and Cooling for Buildings and Industry

Poster

- *Optical and Electrical Characterization of Large Area LSC Systems*
  P. Bernardoni, M. Tonezzer, D. Vincenzi, S. Baricordi, G. Calabrese, V. Guidi
  Proceedings of the 31st European Photovoltaic Solar Energy Conference andExhibition (EUPVSEC 2015), pp. 1492-1493

- *Novel Luminescent Photovoltaic Roof Presented at Versailles during Solar Decahtlon Europe 2014*
  P. Bernardoni, R. Zarcone, M. Tonezzer, D. Vincenzi, M. Brocato, G. Calabrese, V. Guidi, S. Baricordi
  Proceedings of the 31st European Photovoltaic Solar Energy Conference and Exhibition (EUPVSEC 2015), pp. 2909-2910

- *Low concentration solar louvres for building integration*
  D. Vincenzi, F. Aldegheri, S. Baricordi, P. Bernardoni, G. Calabrese, V. Guidi, L. Pozzetti
  9TH International Conference on Concentrator Photovoltaic Systems: CPV-9
  AIP Conference Proceedings, Volume 1556. AIP Conference Proceedings,

Vol.1556, Issue 1, pp. 110-113

Other papers and conference proceedings not related to this thesis work:

Publication

- *Numerical simulation of the temperature distortions in InGaP/GaAs/Ge solar cells working under high concentrating conditions due to voids presence in the solder joint*
  G Calabrese, F Gualdi, S Baricordi, P Bernardoni, V Guidi, L Pozzetti, D. Vincenzi
  Solar Energy 103, 1-11

- *Ge growth on porous silicon: The effect of buffer porosity on the epilayer crystalline quality*
  G Calabrese, S Baricordi, P Bernardoni, D De Salvador, M Ferroni, V Guidi, V Morandi, D Vincenzi
  Applied Physics Letters 105 (12), 122104 (2014)

- *Enhanced reduction in threading dislocation density in Ge grown on porous silicon during annealing due to porous buffer reconstruction*
  Calabrese, G., Baricordi, S., Bernardoni, P., De Salvador, D., Ferroni, M., Guidi, V., Morandi, V., Vincenzi, D.
  Phys. Status Solidi A. doi: 10.1002/pssa.201532427 (2015)

- *Chemoresistive properties of photo-activated thin and thick ZnO films*
  B. Fabbri, A. Gaiardo, A. Giberti, V. Guidi, C. Malagù, A. Martucci, M. Sturaro, G. Zonta, S. Gherardi, P. Bernardoni
  Sensors and Actuators B: Chemical, Volume 222, January 2016, Pages 1251–1256

Oral

- *Towards III-V solar cells on Si: Improvement in the crystalline quality of Ge-on-Si virtual*
  substrates through low porosity porous silicon buffer layer and annealing
  G. Calabrese, S. Baricordi, P. Bernardoni, S. Fin, V. Guidi, D. Vincenzi
  AIP Conference Proceedings, Volume 1616, Issue 1, p.37-40

Poster

- *Development of a new integrated instrument for sun tracking accuracy assessment and DNI measurement*
  F. Aldegheri, S. Baricordi, P. Bernardoni, G. Calabrese, V. Guidi, L. Pozzetti, D. Vincenzi
  CPV-9: International conference on concentrator photovoltaic systems, April 2013, Miyazaki, Japan

- *High and Low Concentration Innovative Solar Systems for Building Integration*
  S. Baricordi, P. Bernardoni, M. Brocato, G. Calabrese, V. Guidi, G. Passerini, L. Pozzetti, M. Tonezzer, D. Vincenzi
  Energy forum – Conference on Advanced Building Skins, November 2013, Bressanone, Italy

8 Appendix A Optical Losses Estimation

The dye molecules inside PMMA have no preferential orientation therefore the light emission from the dyes can be considered isotropic and the emission from each infinitesimal volume of the LSC can be said to have a uniform angular distribution.

If we consider a sphere centred in the infinitesimal LSC volume, the amount of light emitted within a certain angle θ is proportional to the spherical cap subtended by that angle divided by the total surface of the sphere (definition of solid angle).

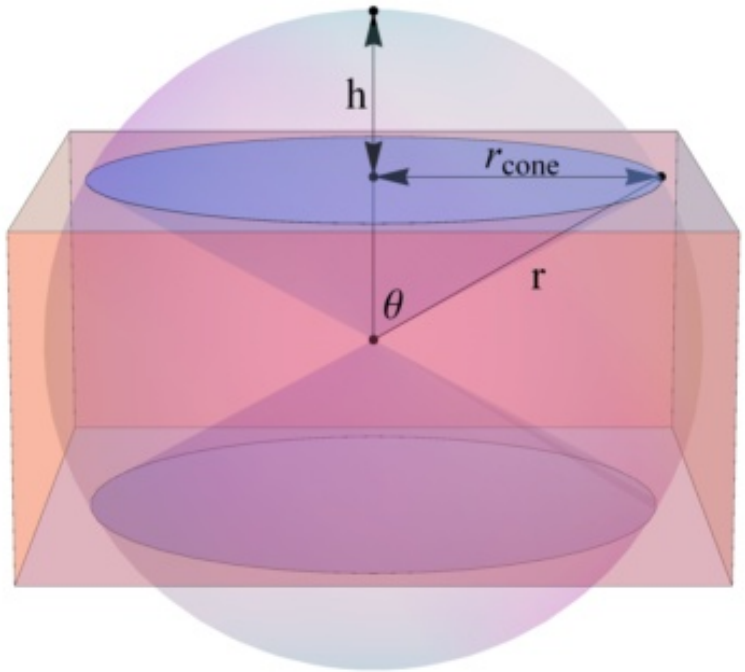

As we know the critical angle depends on the refractive index of the transparent medium with the relationship

$$\theta_{CA} = \arcsin\left(\frac{n_2}{n_1}\right) \overset{air}{=} \arcsin\left(\frac{1}{n_1}\right)$$

Hence if the critical angle is taken as θ the spherical cap is proportional to the light that is non trapped inside the cone by total internal reflection and the cone subtended by this cap is the escape cone.

The escape cone losses are therefore proportional to the surface of the spherical cap subtended by the critical angle.

The expression for the spherical cap surface is

$$S = 2\pi r h = 2\pi r \left[r - r\cos\left(\theta_{CA}\right)\right] = 2\pi r^2 \left[1 - \cos\left(\theta_{CA}\right)\right]$$

Hence the escape cone losses are proportional to the sum of the two escape surfaces S divided by the total surface of the sphere

$$P_{EC} = \frac{4\pi r^2 \left[1 - \cos\left(\theta_{CA}\right)\right]}{4\pi r^2} = 1 - \cos\left(\theta_{CA}\right)$$

substituting the expression for the critical angle yields

$$P_{EC} = 1 - \cos\left(\theta_{CA}\right) = 1 - \cos\left[\arcsin\left(\frac{1}{n}\right)\right] = 1 - \sqrt{1 - \frac{1}{n^2}}$$

while the amount of light trapped inside the LSC

$$P_{IR} = 1 - P_{EC} = \sqrt{1 - \frac{1}{n^2}}$$

9 Appendix B Ocean Optics USB4000-XR1-ES Spectrometer

Specifications	Value
Absolute Maximum Ratings:	
V_{CC}	+5.5 VDC
Voltage on any pin	V_{CC}
Physical Specifications:	
Physical Dimensions	89.1mm x 63.3mm x 34.4mm
Weight	190g
Power:	
Power requirement (master)	230mA at +5 VDC
Supply voltage	4.5 – 5.5V
Power-up time	~5s depending on code size
Spectrometer:	
Design	Asymmetric crossed Czerny-Turner
Focal length (input)	42mm
Focal length (output)	68mm
Input Fibre Connector	SMA 905
Gratings	500 lines/mm
Entrance Slit	25µm slit.
Detector	Toshiba TCD1304AP linear CCD array
Filters	2nd and 3rd order rejection
Spectroscopic:	
Wavelength range	200-1025nm
Integration Time	3.8ms – 10 seconds
Dynamic Range	3.4×10^{6} (system); 1300:1 for a single acquisition
Signal-to-Noise	300:1 (at full signal)
Dark Noise	50 counts RMS
Optical Resolution	~1.7-2.0nm FWHM
Stray Light	<0.05% at 600nm; <0.10% at 435nm
Spectrometer Channels	One
Environmental Conditions:	
Temperature	-30° to +70° C Storage & -10° to +50° C Operation
Humidity	0% - 90% noncondensing
Interfaces:	
USB	USB 2.0, 480 Mbps
RS-232	2-wire RS-232

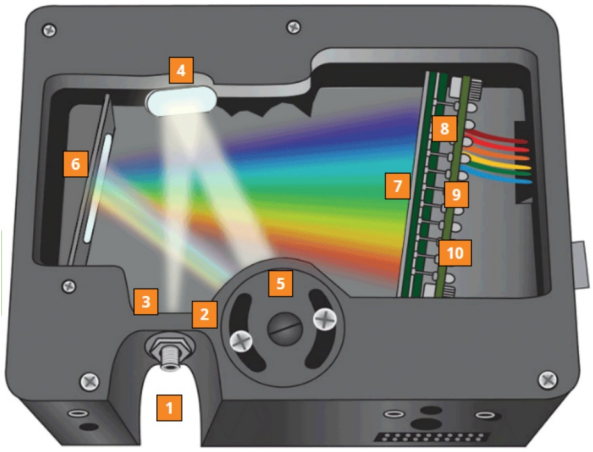

Fig. 9.1: Ocean Optics USB4000-XR1-ES Spectrometer

1. SMA 905 Connector – Secures the input fibre to the spectrometer. Light from the input fibre enters the optical bench through this connector.
2. Slit – A dark piece of material containing a rectangular aperture, which is mounted directly behind the SMA Connector. The size of the aperture (from 5µm to 200µm) regulates the amount of light that enters the optical bench and controls spectral resolution.
3. Filter – Restricts optical radiation to pre-determined wavelength regions. Light passes through the Filter before entering the optical bench. Both bandpass and longpass filters are available to restrict radiation to certain wavelength regions.
4. Collimating Mirror – Focuses light entering the optical bench towards the Grating of the spectrometer. Light enters the spectrometer, passes through the SMA Connector, Slit, and Filter, and then reflects off the Collimating Mirror onto the Grating
5. Grating – Diffracts light from the Collimating Mirror and directs the diffracted light onto the Focusing Mirror. Gratings are available in different groove densities, allowing you to specify wavelength coverage and resolution in the spectrometer.
6. Focusing Mirror – Receives light reflected from the Grating and focuses first-order spectra onto the detector plane.
7. L4 Detector Collection Lens – An optional component that attaches to the Detector to increase light-collection efficiency. It focuses light from a tall slit onto the shorter Detector elements. It should be used with large diameter slits or in applications with low light levels and also improves efficiency by reducing the effects of stray light.
8. Detector (UV or VIS) – Collects the light received from the Focusing Mirror or L4

Detector Collection Lens and converts the optical signal to a digital signal. Each pixel on the Detector responds to the wavelength of light that strikes it, creating a digital response. The spectrometer then transmits the digital signal to the software application.

9. OFLV Filters – OFLV Variable Longpass Order-sorting Filters block second- and third-order light, these filters are optional.
10. UV4 Detector Upgrade – The detector's standard window is replaced with a quartz window to enhance spectrometer performance (<340 nm).

10 Appendix C
Circular Spot and Distance Correction

If we consider the emission evenly distributed across a circle the contribution of each point P within the circle is proportional to the cosine of angle *φ*.

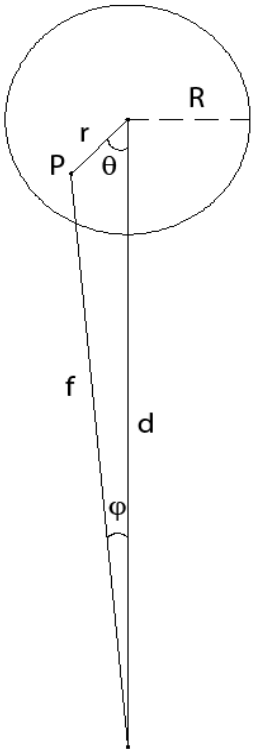

the cosine theorem yield the relationship

$$f^2 = D^2 + r^2 - 2dr\cos(\theta)$$

while for the sine theorem

$$\frac{\sin(\phi)}{r} = \frac{\sin(\theta)}{f}$$

solving for *sin(φ)*

$$\sin(\phi) = \frac{r\sin(\theta)}{f}$$

and using the trigonometric identity $cos^2(x) + sin^2(x) = 1$

$$\cos^2(\phi) = 1 - \frac{r^2\sin^2(\theta)}{f^2}$$

then substituting the expression for *f* previously obtained

$$\cos(\phi)=\sqrt{1-\frac{r^2\sin^2(\theta)}{D^2+r^2-2Dr\cos(\theta)}}$$

this value must be integrated over θ ranging from 0 to π and over r ranging from 0 to R then multiplied by two to consider both the half of the circle, this integral divided by the area of the circle yields the correction factor M

$$M = \frac{2\int_0^R dr\int_0^\pi d\theta\, r\sqrt{1-\frac{r^2\sin^2(\theta)}{D^2+r^2-2Dr\cos(\theta)}}}{\int_0^R dr\int_0^\pi d\theta\, r}$$

This integral has no analytical solution hence the values of *M(D)* were calculated numerically for each distance.

11 Bibliography

[1] A. Goetzberger, W. Greube, Solar energy conversion with fluorescent collectors, 1977, Applied physics A, Vol.14 n.2 pp.123-139

[2] International Energy Agency, Key World Energy Statistics

[3] SunPower, Solar Star Project, 2015, http://us.sunpower.com/utility-scale-solar-power-plants/solar-energy-projects/solar-star-projects/

[4] M. Tonezzer, D. Gutierrez, D. Vincenzi, Solar Cell Nanotechnology, 2013

[5] M. Tonezzer, G. Maggioni, A. Campagnaro, S. Carturan, A. Quaranta, M. Pirriera, D. Gutierrez Tauste, Luminescent solar concentrators employing new Eu (TTA) 3phen-containing parylene films, Progress in Photovoltaics: Research and Applications, Vol.23 n. pp.1037-1044

[6] R. H. Inman, G. V. Shcherbatyuk, D. Medvedko, A. Gopinathan, S. Ghosh, Cylindrical luminescent solar concentrators with near-infrared quantum dots, 2011,Optics Express, Vol.19 n.24 pp.24308-24313

[7] Y. Jingli, G. Wang, Lanthanide Complex-Based Fluorescence Label for Time-Resolved Fluorescence Bioassay, 2005, Journal of Fluorescence, Vol.15 n.4 pp.559-568

[8] M. Tonezzer, G. Maggioni, A. Campagnaro, S. Carturan, A. Quaranta, M. Pirriera, D. Gutierrez Tauste, Luminescent solar concentrators employing new Eu(TTA)3phen-containing parylene films, 2015, Progress in Photovoltaics: Research and Applications, Vol.23 n.8 pp.1037-1044

[9] M.A. Reed, J.N. Randall, R.J. Aggarwal, R.J. Matyi, T.M. Moore, A.E. Wetsel, Observation of discrete electronic states in a zero-dimensional semiconductor nanostructure, 1988, Physical Review Letters, Vol.60 n.6 pp.535-537

[10] Anglo Adhesives & Services Ltd., Technical Data Sheet: Anglosol Cement 700,

[11] DELO Industrial Adhesives, Technical Data Sheet: DELO-PHOTOBOND GB368, 2014

[12] 3M, Technical Data Sheet: DF2000MA Release B, 2015

[13] BASF Corporation, Lumogen F Yellow 083 Datasheet

[14] BASF Corporation, Lumogen F Orange 240 Datasheet

[15] BASF Corporation, Lumogen F Red 305 Datasheet

[16] M. Ebert, T. Fellmeth, T. Dörsam, F. Clement, D. Biro, M. Wiesenfarth, U. Eitner, A Low Concentrating Cell and Receiver Concept Based onLow Cost Silicon Solar Cells, 2015, 11th International Conference on Concentrator Photovoltaic Systems: CPV11, Vol.1679 n. pp.110001

[17] F. Aldegheri, S. Baricordi, P. Bernardoni, M. Brocato, G. Calabrese, V. Guidi, L. Mondardini, L. Pozzetti, M. Tonezzer, D. Vincenzi, Building integrated low concentration solar system for a self-sustainable Mediterranean villa: The Astonyshine house, 2014,

Energy and Buildings, Vol. n.77 pp.355-363

[18] W. H. Weber, J. Lambe, Luminescent greenhouse collector for solar radiation, 1976, Applied Optics, Vol.15 n.10 pp.2299-2300

[19] W. G. van Sark, Z. Krumer, C. De Mello Donega, R. E. I. Schropp, Luminescent Solar Concentrators: The route to 10% efficiency, 2014, IEEE 40th Photovoltaic Specialist Conference (PVSC), Vol. n.30 pp.2276-2279